RESEARCH ARTICLE

N-glycosylation of the protein disulfide isomerase Pdi1 ensures full *Ustilago maydis* virulence

Miriam Marín-Menguiano☯, **Ismael Moreno-Sánchez**[ID]☯, **Ramón R. Barrales**[ID], **Alfonso Fernández-Álvarez**[ID]*, **José Ignacio Ibeas**[ID]*

Centro Andaluz de Biología del Desarrollo (CABD), Universidad Pablo de Olavide-Consejo Superior de Investigaciones Científicas-Junta de Andalucía, Ctra. Utrera km.1, Seville, Spain

☯ These authors contributed equally to this work.
* aferalv@upo.es (AFA); joibecor@upo.es (JII)

Abstract

Fungal pathogenesis depends on accurate secretion and location of virulence factors which drive host colonization. Protein glycosylation is a common posttranslational modification of cell wall components and other secreted factors, typically required for correct protein localization, secretion and function. Thus, the absence of glycosylation is associated with animal and plant pathogen avirulence. While the relevance of protein glycosylation for pathogenesis has been well established, the main glycoproteins responsible for the loss of virulence observed in glycosylation-defective fungi have not been identified. Here, we devise a proteomics approach to identify such proteins and use it to demonstrate a role for the highly conserved protein disulfide isomerase Pdi1 in virulence. We show that efficient Pdi1 N-glycosylation, which promotes folding into the correct protein conformation, is required for full pathogenic development of the corn smut fungus *Ustilago maydis*. Remarkably, the observed virulence defects are reminiscent of those seen in glycosylation-defective cells suggesting that the N-glycosylation of Pdi1 is necessary for the full secretion of virulence factors. All these observations, together with the fact that Pdi1 protein and RNA expression levels rise upon virulence program induction, suggest that Pdi1 glycosylation is important for normal pathogenic development in *U. maydis*. Our results provide new insights into the role of glycosylation in fungal pathogenesis.

Author summary

Fungal pathogens require virulence factors to be properly secreted and localized to guarantee complete infection. In common with many proteins, virulence factors must be post-translationally modified by glycosylation for normal localization, secretion and function. This is especially important for virulence factors, which are mainly comprised of cell wall and secreted proteins. Aberrant glycosylation leads to a loss of virulence in both animal and plant pathogenic fungi. We have previously demonstrated that glycosylation is important for virulence of the corn smut fungus, *Ustilago maydis*. However, the glycoproteins

involved and their specific roles in the infection process have not yet been reported. Here, we describe a proteomic assay designed to identify glycoproteins involved in plant infection. Using this method, we define the role of Pdi1 protein disulfide isomerase in virulence. Interestingly, abolishing Pdi1 N-glycosylation mimics Δ*pdi1* defects observed during infection, suggesting that Pdi1 N-glycosylation is required for the normal secretion of virulence factors. We hypothesize that Pdi1 N-glycosylation is necessary for maintaining proper effector protein folding during the infection process, especially in the harsh conditions found inside the maize plant.

Introduction

Protein glycosylation is a common eukaryotic post-translational mechanism required for the correct folding, activity and secretion of many proteins. Glycosylation involves the synthesis and addition of different polysaccharide cores (sugars) to specific amino acids within a consensus sequence. Most glycoproteins are plasma membrane-associated cell wall and secreted proteins, which acquire glycosyl groups during their transit through the Endoplasmic Reticulum (ER) and Golgi Apparatus (GA) [1,2]. Defects during the synthesis or addition of sugars to target proteins affect many biological processes; for instance, impaired human protein glycosylation causes more than 100 severe embryonic development disorders [3]. In pathogenic fungi, glycosylation defects lead to a reduction or absence of virulence in plant and animal pathogens [4–8].

Protein glycosylation is divided into different types based on the structure and composition of the oligosaccharide cores and the amino acids to which they are attached. N- and O-glycosylation are the most common types in pathogenic fungi. N-glycosylation consists of the addition of an oligosaccharide core, composed of two N-acetylglucosamines (NAcGlc), nine mannoses (Man) and three glucose (Glc) molecules, $NAcGlc_2Man_9Glc_3$, to the nitrogen chain of an asparagine residue in the sequence Asn-*x*-Ser/Thr, where *x* can be any amino acid except proline [9,10]. O-glycosylation is more variable than N-glycosylation in terms of the types of sugars added. In fungi O-mannosylation is the most common type of O-glycosylation and is characterized by the addition of Man residues to target proteins. In contrast to N-glycosylation, O-glycosylation involves sequential additions of Man to the oxygen chain of Ser or Thr amino acids although no amino acid consensus sequence has been identified [11]. N- and O-linked glycans are later processed during their transit across the ER and GA, and specific trimming of sugars is also essential for the function and secretion of glycoproteins [5,12].

Crucial components for fungal pathogenesis belonging to N- and O-glycosylation pathways have been identified in several organisms such as *Candida albicans*, *Aspergillus nidulans*, *Cryptococcus neoformans*, *Magnaporthe oryzae* or *Ustilago maydis* [4,6–8,13–15]. The loss of these proteins primarily affects those stages of pathogenic development that require robust glycoprotein secretion. The involvement of protein glycosylation in fungal virulence has been extensively explored in the corn smut fungus *U. maydis* [4,5,16].

U. maydis combines both pathogenic and non-pathogenic phases during its life cycle. During the non-pathogenic stage, *Ustilago* grows as haploid yeast-like cells that can be easily cultured in the laboratory. The pathogenic phase starts when two sexually compatible strains mate on the maize plant surface. Sexual compatibility is determined by two independent loci: *locus a*, which encodes a pheromone-receptor system; and *locus b*, which encodes a transcription factor formed by a *bE/bW* heterodimer. Formation of the *bE/bW* complex triggers development of an infective dikaryon filament [17]. Physical and chemical plant signals are sensed

by filaments that develop a morphogenetic structure called the appressorium, which mediates plant cuticle penetration [18]. Once inside plant tissues, the fungus expands in a branched filamentous form generating hypertrophied plant cells, macroscopically visible as tumors [19–23].

N- and O-glycosylation are both crucial for *U. maydis* pathogenic development. The loss of the O-mannosytransferase Pmt4, which catalyzes the addition of mannoses to target proteins, compromises both appressorium formation and plant cuticle penetration. Hence, Δ*pmt4* cells are unable to invade the plant tissues and tumor induction is fully abolished [4]. Glucosidase I and II (Gls1 and Gas1/Gas2) are important for N-glycan processing in the ER and play crucial roles during the early stages of *U. maydis* plant colonization [5,8]. A reasonable explanation for these drastic virulence defects is that deficient glycosylation could greatly alter the location and/or function of glycoproteins involved in virulence, and consequently compromise multiple stages of *U. maydis* pathogenic development such as plant cuticle penetration, fungal progression inside plant tissues or plant defense responses. Despite the importance of Pmt4 and Gls1 for maize infection, the virulence factors glycosylated by these proteins are still poorly described. In this context, an *in silico* search for putative Pmt4 targets identified Msb2 as an O-glycoprotein, whose deletion causes virulence defects that resemble some of those described for the Δ*pmt4* mutant [16]. However, a more wide-ranging approach is required to find new glycosylated virulence factors.

In this work we devise a proteomics approach designed to identify N- and O-glycoproteins produced when the infection program is activated. Using this method, we identify several Gls1 and Pmt4 targets involved in virulence. Among these, we further characterize Pdi1, a disulfide isomerase protein whose glycosylation we demonstrate to be required for full virulence in maize plants due to its involvement in glycoprotein folding. Furthermore, we show that the deletion of Pdi1 affects glycoprotein secretion in *U. maydis*. We speculate about its role during the infection process, which could be related to ensuring the effective production and secretion of many virulence factors.

Results

Glycoproteomic screening for Pmt4 and Gls1 substrates

Previous work from our laboratory has shown that the *U. maydis* proteome contains a high number of putative O-glycoproteins mannosylated by the O-mannosyltransferase Pmt4 [16]. An *in silico* screen for proteins harboring Ser/Thr-rich regions, where Pmt4 attaches mannoses, revealed that around 65% of *U. maydis* proteins are potential O-glycosylation targets [16]. If proteins containing N-glycosylation sites are included, this number rises to over 70% of the proteome, suggesting a potential role for protein glycosylation in the activity of a high proportion of *U. maydis* proteins (S1 Fig). In order to identify virulence-related glycosylation targets, we designed a selective glycoproteomic screen based on the hypothesis that glycoproteins whose expression is modified upon virulence program induction are likely to have important roles in the pathogenic phase of the *U. maydis* life cycle.

For this screen we set out to analyze cell extracts corresponding to cytosolic, cell wall and secreted proteins using two-dimensional differential gel electrophoresis (2D-DIGE) to detect glycoproteins whose spot area or intensity were altered by the loss of Pmt4 or Gls1 and corresponding effect on O- or N- glycosylation activities, respectively. To isolate glycoproteins from cytosolic extract and avoid interference with other proteins, total protein extracts were enriched for mannose-containing proteins by Fast-Performance Liquid Chromatography (FPLC) using *Concanavalin A* columns (Fig 1). Due to the high proportion of glycoproteins in cell wall and secreted extracts, FPLC enrichment was not applied to these preparations. The loss of *biz1* leads to severe defects in appressoria development and penetration [24], which are
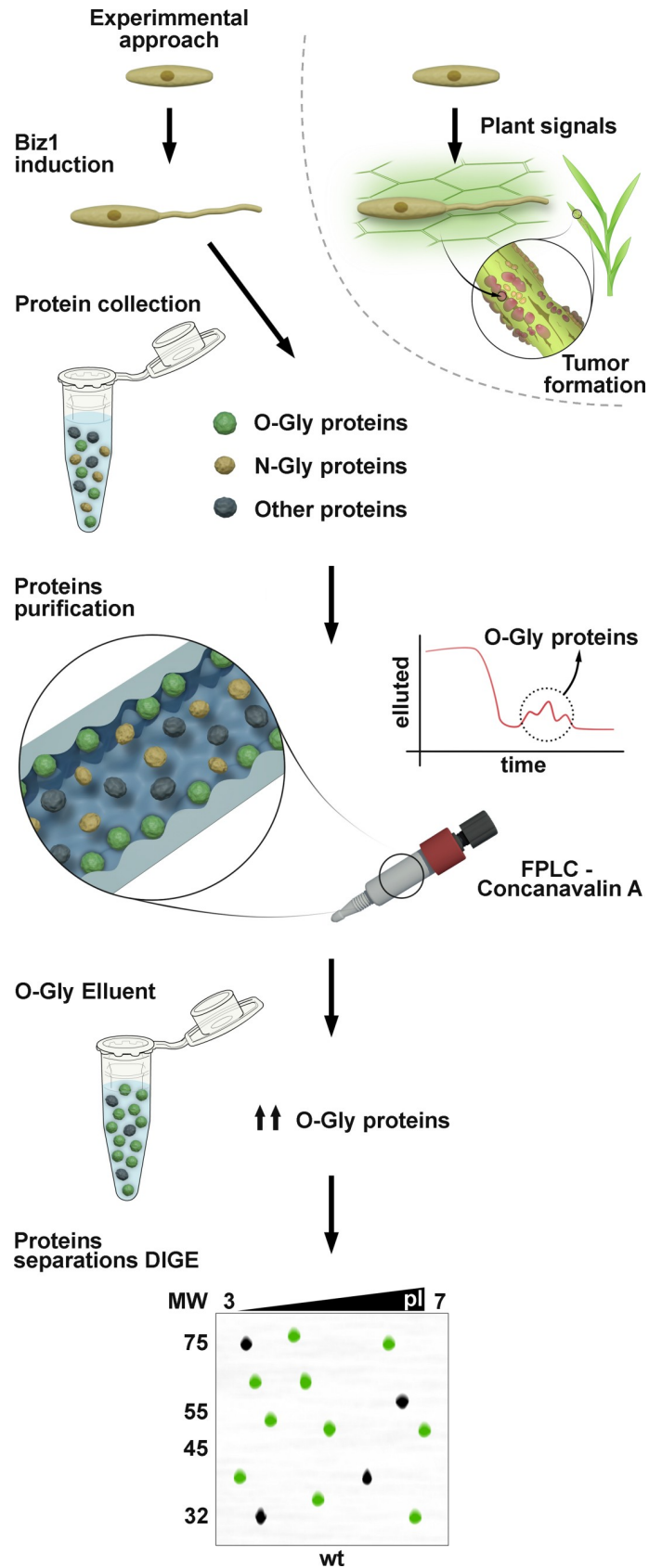
Fig 1. Proteomic approach to identify glycoproteins involved in virulence. Cytosolic proteins were collected from FB1 wild-type *U. maydis* and from a mutant deficient in either O- or N- glycosylation upon Biz1 repression or induction conditions. O- or N-glycoproteins are purified through a Concanavalin A FPLC column using O- or N-glycoprotein specific eluents. Finally, glycoproteins are tagged with fluorophores and separated by 2D electrophoresis.

reminiscent of the phenotypes observed in Δ*pmt4* and Δ*gls1* maize infections [4,5]. *biz1* encodes a *b*-dependent zinc-finger protein whose induction activates pathogenic filamentous growth [24]. Hence, we hypothesized that effectors controlled by Biz1 might require glycosylation mediated by Pmt4 and/or Gls1. To test this, we expressed *biz1* under the control of the carbon source-regulated P_{crg} promoter that is induced by arabinose (*biz ON*) and repressed by glucose (*biz OFF*) [24,25]. Thus, FB1 wild-type (*wt*), Δ*pmt4* and Δ*gls1* cells harboring P_{crg} controlled-*biz1* were collected under inducing and repressing conditions and protein samples compared, using three replicas of each, to identify the differentially migrating proteins ([Fig 1]).

By applying the approach described above, we detected protein spots whose areas showed altered electrophoretic mobility compared to *wt* in a Biz1-dependent manner in both Δ*pmt4* and Δ*gls1* cells, presumably corresponding to O- and N-glycoproteins respectively. Using Matrix-Assisted Laser Desorption/Ionization–Mass Spectrometry (MALDI–MS) we identified four proteins in the cytosolic extract with altered mobility in both mutants that probably correspond to both O- and N-glycosylated proteins: the chorismate mutase Cmu1, the α-L-arabino-furanosidase Afg1, the invertase Suc2 and UMAG_10156, a putative disulfide-isomerase ([Fig 2]). In addition, we identified 23 N- or O-glycoproteins from the cytosolic extract, 6 from the cell wall extract and 11 from the secreted extract showing electrophoretic mobility changes ([Fig 3], [S1 Table]). Of the proteins identified only Cmu1, UMAG_04926 (Pep4), Afg1 and UMAG_04309 (Afg3) have been previously characterized. Cmu1 is a secreted virulence factor that controls the metabolic status of plant cells during fungal colonization; deletion of *cmu1* reduces *U. maydis* virulence in the solopathogenic strain CL13 [26]. Pep4 is a proteinase A located at the vacuole, which is involved in the yeast to micelium dimorphic transition and whose deletion causes reduced virulence including incomplete teliospore maturation [27]. On the other hand, Afg1 and Afg3 are arabinofuranosidases that participate in the degradation of arabinoxylan, a plant cell wall component. While the loss of *afg1* or *afg3* is dispensable for virulence, the triple deletion of *afg1*, *afg2* and *afg3* compromises full pathogenic development [28]. The involvement of the other identified proteins in pathogenesis remains to be determined.

The disulfide-isomerase Pdi1 is a substrate of Pmt4 and Gls1, and Pdi1 is required for pathogenesis

To determine the involvement in pathogenesis of the uncharacterized proteins, we compared the virulence capability of CL13 strain mutants carrying deletions corresponding to several of the candidate proteins. The CL13 strain harbors genes encoding a compatible *bE1/bW2* heterodimer allowing it to complete full pathogenic development [29]. Analysis of disease symptoms after infection revealed strong virulence defects in Δ*afg1*, Δ*UMAG_00309*, Δ*UMAG_02751*, Δ*UMAG_03416*, Δ*UMAG_04180*, Δ*UMAG_04422*, Δ*UMAG_04733*, Δ*UMAG_05223*, Δ*UMAG_10156*, and Δ*UMAG_11496* infections ([Fig 4A], [S2 Fig] and [S1 Table]). Candidate genes were then tested in more virulent strains; the wild type FB1 and FB2 strains [30], which have a higher infection capacity, and SG200, which carries the *mfa2* gene that encodes the compatible mating type pheromone [29] and confers stronger virulence. Based on the virulence assays in these backgrounds we identified UMAG_10156 as having the most significant role in plant infection ([Fig 4B, 4C and 4D]). Blast analysis for UMAG_10156 revealed 36% identity to *Saccharomyces cerevisiae* Pdi1 with 48% and 43% identity in the two thioredoxin
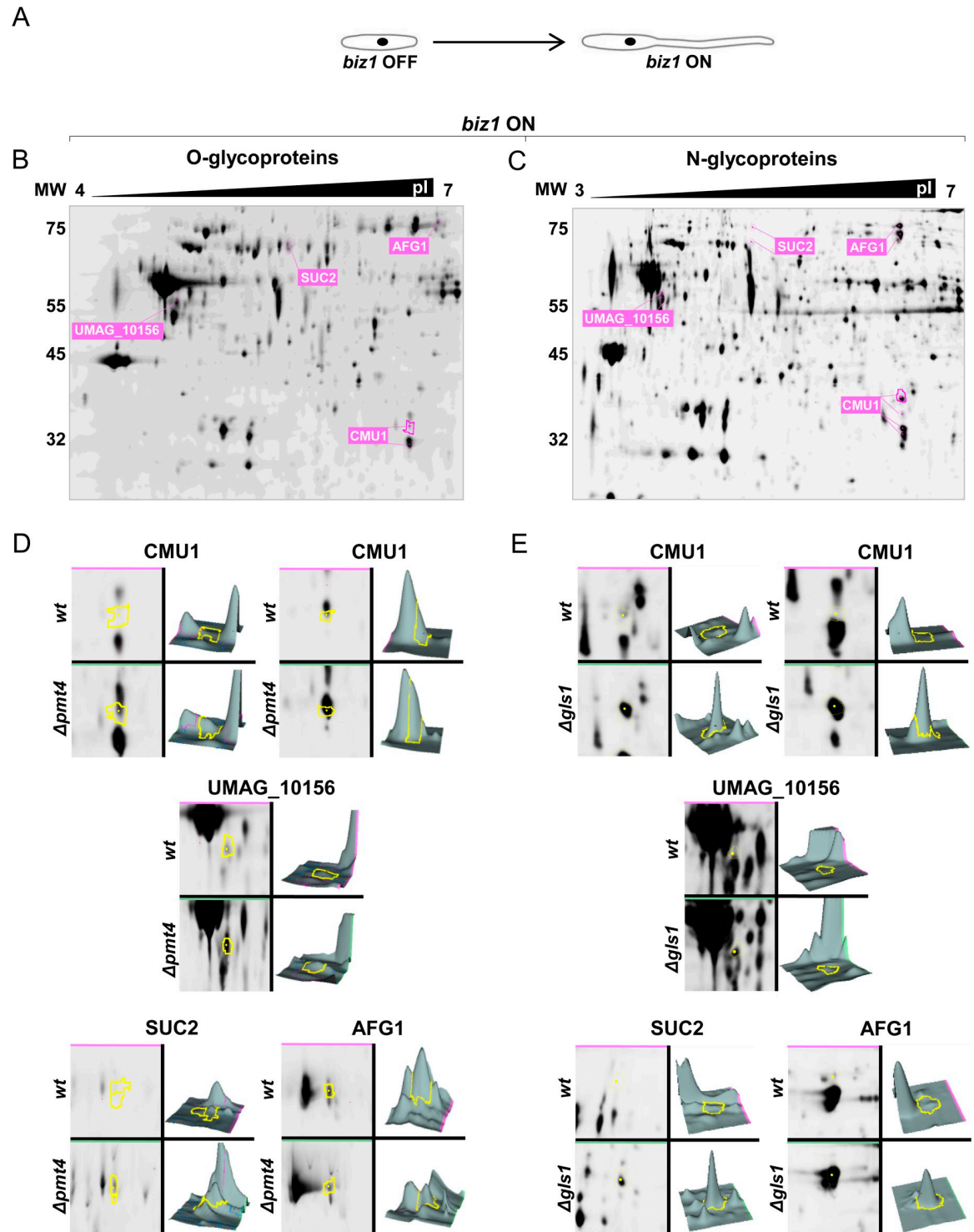
Fig 2. 2D-DIGE expression analysis of Pmt4 and Gls1- dependent cytoplasmic glycoproteins. Cells growing in inducing conditions develop hyphae (A). Images of DIGE gels containing an internal standard loaded with equal amounts of each sample, showing protein changes between *biz1* and *pmt4*-mutants (B) or *biz1* and *gls1*-mutants (C). Protein expression profile changes between wild-type *biz1^{crg}* vs Δ*pmt4* mutants (D) or Δ*gls1* mutants (E) showed by the DeCyder software analysis. The edge of the indicated protein is displayed in the DIGE gel in pink and in a specific zoom in yellow.

A

B
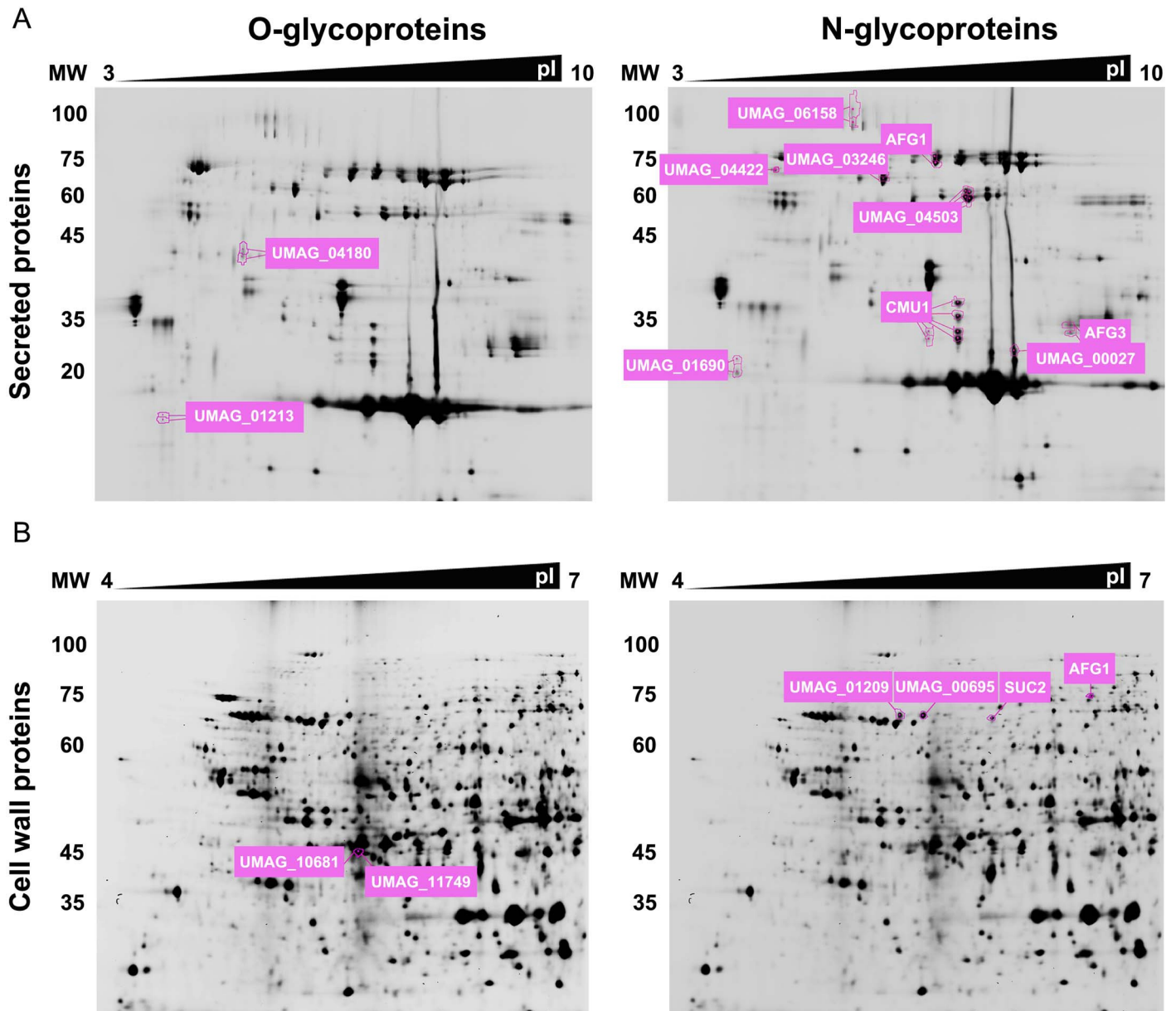
Fig 3. 2D-DIGE expression analysis of Pmt4 and Gls1- dependent secreted or cell wall glycoproteins. Images of the DIGE gels containing an internal standard loaded with equal amounts of each samples, showing protein changes between wild-type *biz1^crg* and *pmt4*-mutants (secreted glycoproteins in A, left part; cell wall glycoproteins in B, left part) or wild-type *biz1^crg* and *gls1*-mutants (A, right part; B right part).

https://doi.org/10.1371/journal.ppat.1007687.g003

domains (Fig 5A and S3 Fig). Thus, we will now refer to UMAG_10156 as Pdi1 for the remainder of the article. *S. cerevisiae* Pdi1 is a disulfide-isomerase protein, member of the thioredoxin superfamily of redox proteins whose canonical role is to support the folding of newly synthesized proteins in the ER *via* the addition of disulfide bonds [31].

The loss of Pdi1 compromises fungal expansion inside plant tissues

Previous studies in budding yeast have shown that Pdi1 function is critical under ER stress conditions, where a large number of misfolded proteins are produced [32,33]. To confirm that this function of Pdi1 is retained in *U. maydis*, we explored Pdi1 localization and studied the
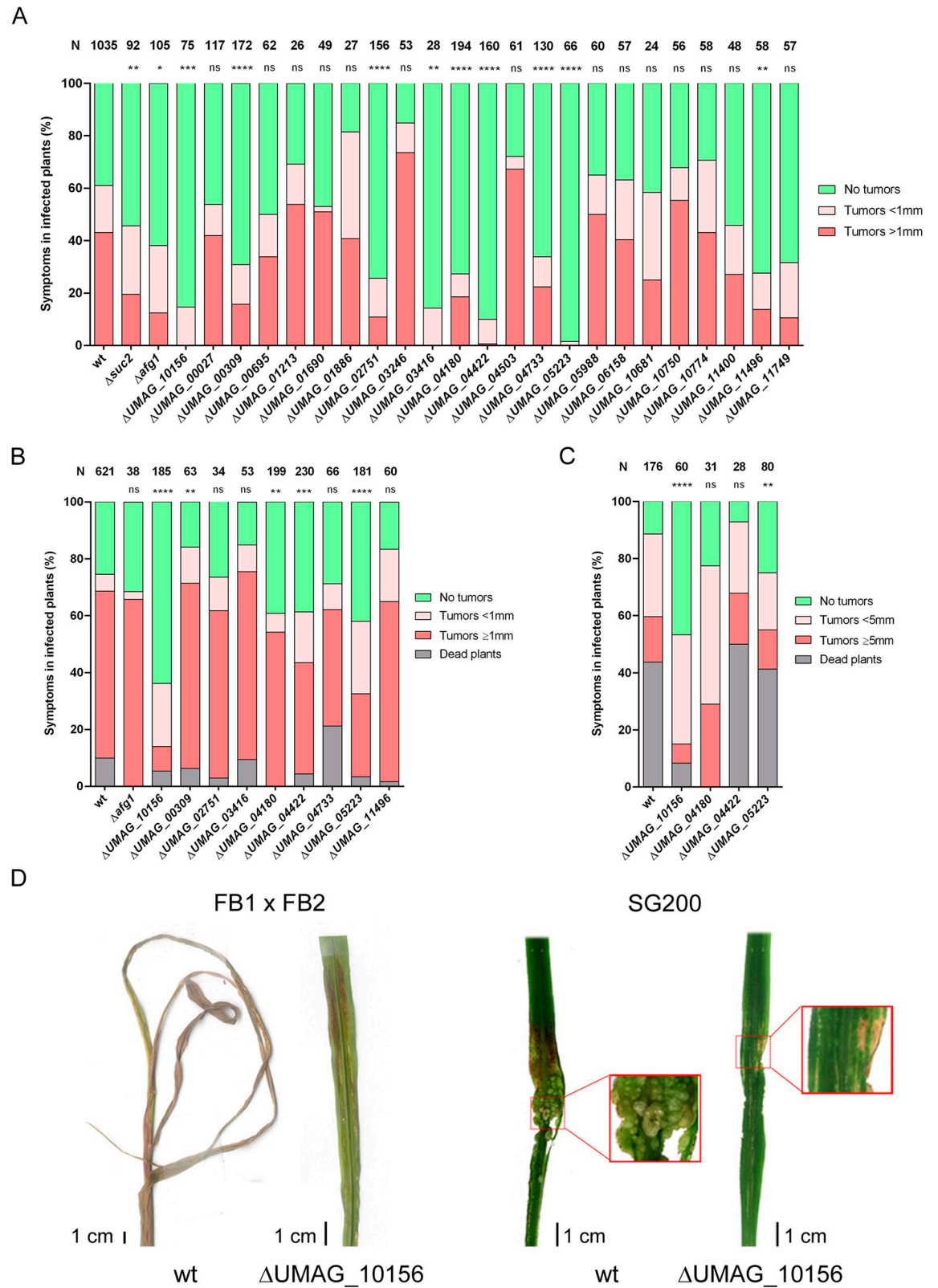
Fig 4. Infection assay of pathogenic pathway glycoprotein candidates. Deletions and infections were first carried out in the CL13 strain (A). Deletions showing a statistically significant reduction in virulence were then assayed in SG200 (B) and subsequently in FB1 and FB2 compatible strains (C). Total number of plants infected is indicated above each column. The indicated number of plants for

wild-type infections is the sum of all wild-type infected plants in each mutant virulence assay (see S2 Fig for infection experiments listing single deletions with their own corresponding wild-type dataset). The Mann-Whitney statistical test was performed for each mutant versus the corresponding wild-type strain (ns: not statistically significant; * for p-value < 0.05; ** for p-value < 0.01; *** for p-value < 0.005; **** for p-value < 0.0001). (D) Representative Δ*UMAG_10156* disease symptoms compared to wild-type.

https://doi.org/10.1371/journal.ppat.1007687.g004

ability of Δ*pdi1* cells to grow under reductive ER stress induced by dithiothreitol (DTT). Microscopy co-localization analysis of Pdi1:GFP and the ER marker mRFP:HDEL confirmed the localization of Pdi1 to this organelle (Fig 5B), where it has been shown to work in conjunction with Calnexin and Calreticulin in the refolding of glucosidated proteins [34]. Moreover, Δ*pdi1* cells showed a hypersensitivity response to DTT, thus confirming the canonical role of Pdi1 in *U. maydis* (Fig 5C and 5D).

To identify the causes behind the failure of Δ*pdi1* plant infections we first analyzed if the *pdi1* deletion causes growth alterations under axenic conditions. We found no differences in generation time (~2.5 hours in rich media) (S4A Fig) or cell morphology (S4B Fig) between *wt*
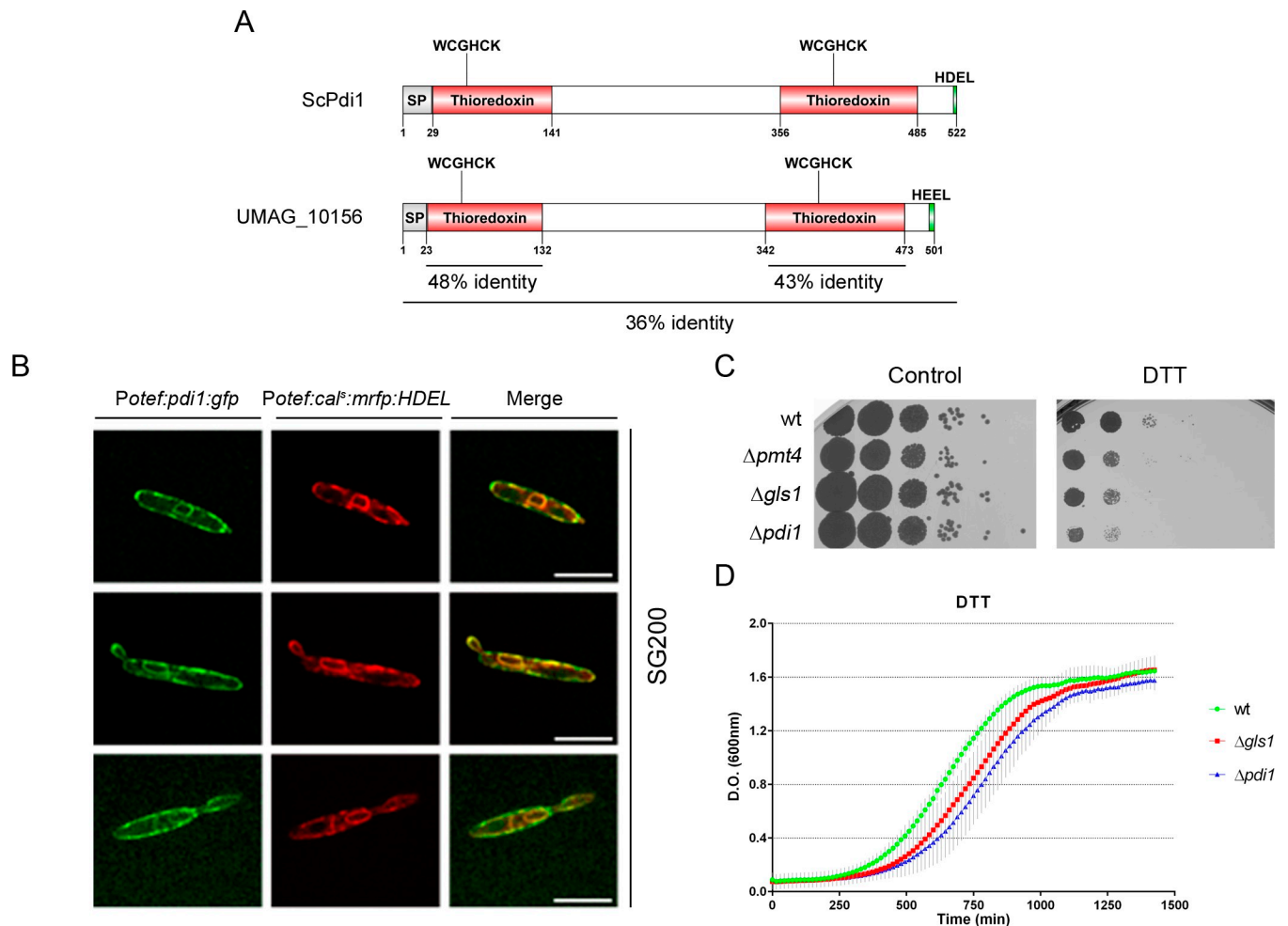
Fig 5. Pdi1 (UMAG_10156) is a protein disulfide isomerase that localizes to the ER and its deletion results in sensitivity to ER stress inducing treatments. (A) Schematic representation of ScPdi1 and UMAG_10156 showing signal peptides (SP), thioredoxin domains, WCGHCK active sites, HDEL/HEEL ER localization sites and thioredoxin domain and whole protein identity percentages obtained by BLASTp. (B) Pdi1:GFP co-localizes with the ER marker mRFP:HDEL. Scale bar represents 5 μm. (C) ER stress assay was performed on solid CM plates supplemented with 2% D-glucose and 4 mM DTT. (D) ER stress assay performed with liquid media supplemented with 10 mM DTT.

https://doi.org/10.1371/journal.ppat.1007687.g005

and Δ*pdi1* cells. Moreover, Δ*pdi1* did not show any defects in cell wall integrity or oxidative stress resistance (S5 Fig). Next, we examined if the mating capability between sexually compatible cells depends on Pdi1. This can be tested by analyzing dikaryon filament formation on charcoal plates, which are recognizable by the formation of white fuzzy colonies. We observed similar mating efficiency in FB1Δ*pdi1* and FB2Δ*pdi1* crosses compared to the *wt* strains (Fig 6A). Therefore, the pathogenic defects affecting Δ*pdi1* infections are probably not caused by failures in cellular growth or mating stages. Hence, the plant infection defects observed in *pdi1* mutant cells probably appear during interaction with the host. In fact, we have observed an increase in both Pdi1 protein levels upon *biz1* activation and *pdi1* transcription during the infection process, with a peak at three days post infection (dpi) (Fig 6B and 6C), in agreement with a high-throughput transcriptomic analysis of pathogenesis [35]. These observations suggest that Pdi1 function is required during the plant infection process, possibly to ensure the correct folding of the increased quantity of glycosylated and secreted proteins that must be expressed for a successful infection to develop.

To determine which step of *U. maydis* pathogenic development is affected by the loss of Pdi1, we analyzed the behavior of Δ*pdi1* cells during plant cuticle pre-penetration stages. A physicochemical plant signal is recognized by the fungal cell, triggering filamentous growth and appressoria formation [18]. In order to quantify both phenotypes, we generated the *pdi1* deletion in SG200 cells carrying RFP under the control of the constitutive *otef* promoter and co-inoculated maize plants with an equal mixture of SG200 P*otef*GFP and SG200 P*otef*RFP Δ*pdi1* cells. The amount of filaments and appressoria in *wt* and Δ*pdi1* cells was quantified using fluorescence microscopy ~15 hours after infection. We found that the absence of Pdi1 did not alter filament formation capability (Fig 6D). Moreover, Δ*pdi1* filaments developed appressoria normally (Fig 6E). Thus, plant penetration stages do not require Pdi1, which suggests that deficient fungal expansion inside plant tissues might be behind the Δ*pdi1* infection defects.

To address the state of fungal colonization inside plant tissues we stained infected maize leaves 3 and 5 days after inoculation using Wheat Germ Agglutinin (WGA)-Alexa and propidium iodide to visualize fungal hyphae and plant cells, respectively (see Methods). Following this approach, we observed a defective proliferation of Δ*pdi1* hyphae inside the plant (Fig 6F). To confirm these observations, we quantified fungal biomass in plant samples. We used the expression level of the *U. maydis ppi1* gene as a fungal marker [36]. We found that the amount of fungal biomass 3 days post-infection decreased two-fold during Δ*pdi1* infection versus infection with a *wt* strain (Fig 6G). Thus, Pdi1 plays a key role in *U. maydis* colonization after plant penetration. Interestingly, this phenotype is reminiscent of defects caused by N-glycosylation defective cells [5] suggesting that altered Pdi1 function might be partly responsible for the defects associated with the loss of N-glycosylation.

Loss of Pdi1 N-glycosylation mimics Δ*pdi1* virulence defects

An important remaining question is whether the loss of Pdi1 glycosylation mediated by Pmt4 and Gls1 leads to dysfunctional Pdi1 and a reduction in virulence similarly to Δ*pdi1* cells, or alternatively, a non-glycosylated Pdi1 form is still able to induce plant tumors and Pmt4 and Gls1 affect virulence elsewhere. To address this issue, putative O- and N-glycosylation sites were substituted with alanine (S4A, S24A, S340A, S344A, S346A, S350A, S477A and T486A) and glutamine (N36Q and N484Q) residues, respectively (Methods, Fig 7A). Pdi1 alleles harboring substitutions at all O-glycosylation sites (Pdi1$^{\Delta O\text{-gly}}$), all N-glycosylation sites (Pdi1$^{\Delta N\text{-gly}}$), all O- and N-glycosylation sites (Pdi1$^{\Delta N,O\text{-gly}}$) or the wild type allele were introduced as single copies in the exogenous *ip* locus of Δ*pdi1* cells under the control of the *pdi1* promoter and their ability to infect maize plants tested. We found that while Pdi1$^{\Delta O\text{-gly}}$
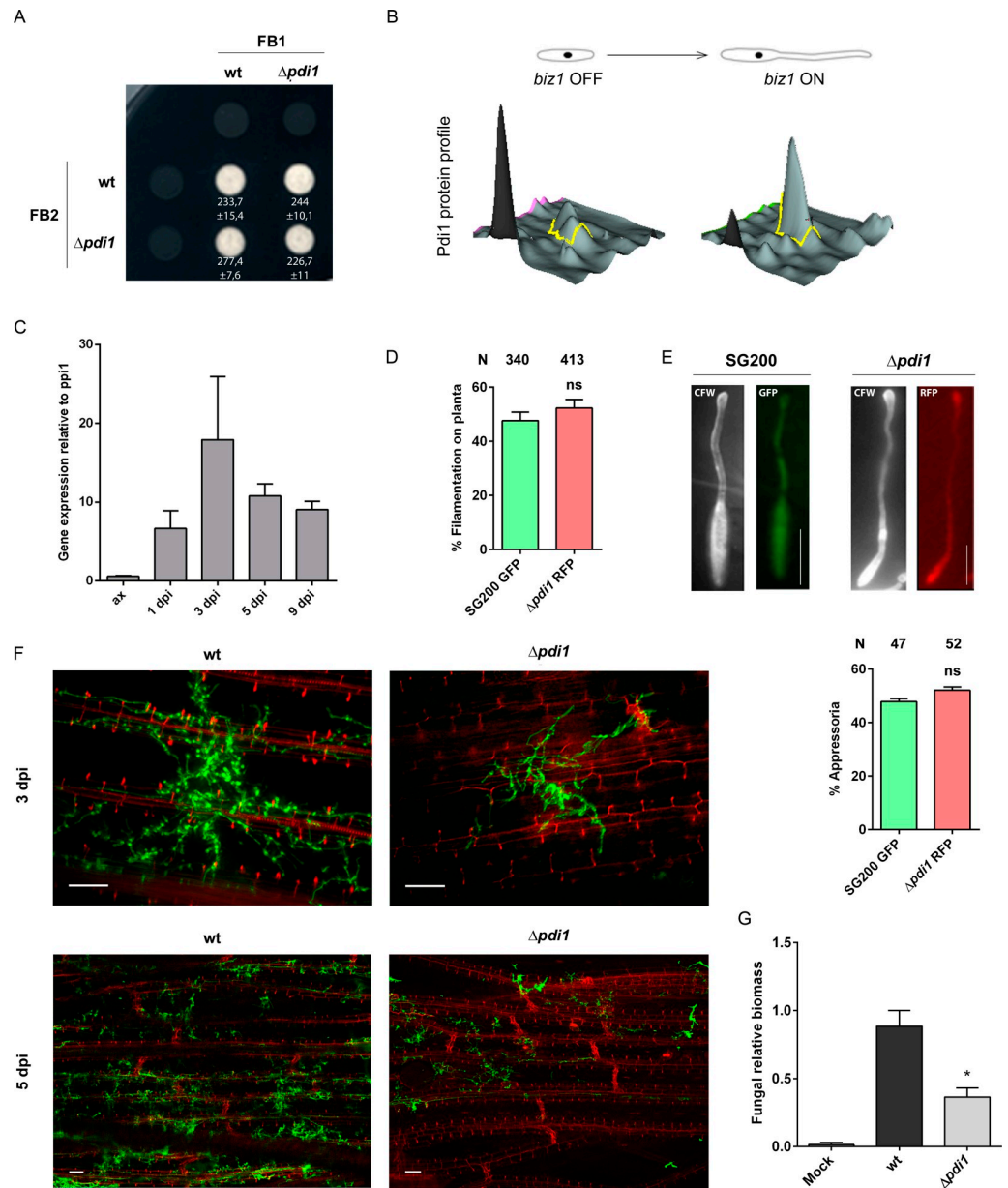
Fig 6. Pdi1 is essential for fungal growth within the maize plant. (A) Mating assay between compatible *U. maydis* strains, FB1 and FB2 Δ*pdi1* were tested on PD-charcoal (PD-Ch) plates. (B) Pdi1 protein expression profile before and after *biz1* activation obtained by DiGE analysis. (C) *pdi1* expression levels relative to *ppi1* during maize plant infection calculated by qRT-PCR from RNA isolated from plants infected with FB1 x FB2 at 1, 3, 5 and 9 days post infection and RNA from axenic culture. Maize seedlings were co-infected with SG200 GFP and SG200 Δ*pdi1* RFP strains. After 15h, filament (D) and appressoria (E) formation were measured by scoring for GFP or RFP fluorescence. Total number of plants infected is indicated above each column. Scale bar represents 5 μm. (F) Maize leaves from 3 and 5 dpi plants infected with SG200 and SG200Δ*pdi1* were stained with propidium iodide (red) and *U. maydis* hyphae with WGA-AF-488 (green), and visualized by fluorescence microscopy, showing a decrease in the growth and branching capability of the *pdi1* mutant. Scale bar represents 50 μm. (G) Quantification of fungal biomass *in planta* at 3 dpi was performed by qPCR, measuring the constitutively-expressed *ppi1 U. maydis* gene normalized to the constitutively-expressed plant *gapdh* gene, confirming its defective proliferation. T-test statistical analysis was performed (* for *p*-value < 0.05).
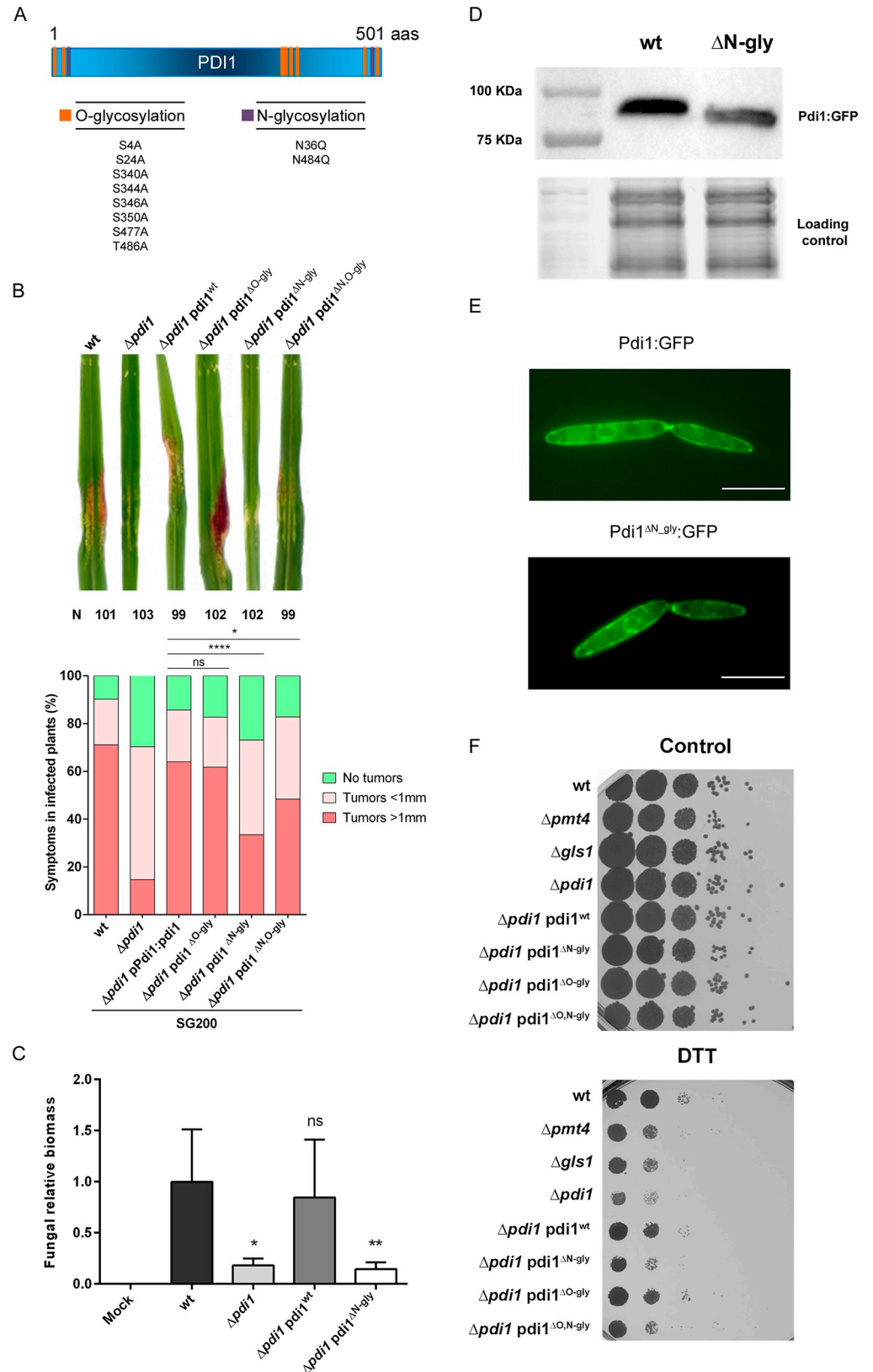
Fig 7. N-glycosylation of the protein disulfide isomerase Pdi1 ensures *U. maydis* virulence. (A) Pdi1 has two putative N-glycosylation sites and eight putative O-glycosylation sites. The main amino acids where the glycosylation

tree is anchored, serine/threonine in O-glycosylation and asparagine in N-glycosylation, have been replaced by similar amino acids alanine and glutamine for O- and N-glycosylation, respectively. (B) The percentage of symptoms in maize plants infected with the indicated strains at 14 dpi. Three independent infections with around 30 plants each were performed, and the total number of infected plants is indicated above each column. The Mann-Whitney statistical test was performed pooling the data for the three independent experiments (ns: not statistically significant; * for p-value < 0.05, **** for p-value < 0.001) or individually for each experiment as shown in S4 Table. Representative disease symptoms are shown above. (C) Quantification of fungal biomass *in planta* at 5 dpi was performed by qPCR, measuring the constitutively-expressed *ppi1 U. maydis* gene normalized to the constitutively-expressed plant *gapdh* gene. T-test statistical analysis was performed (ns for not statistically significant, * for p-value < 0.05, ** for p-value < 0.01). (D) Western blot showing Pdi1:GFP in SG200 and Pdi1$^{\Delta\text{N-gly}}$: GFP in SG200 $\Delta pdi1$, with the image of the stain-free gel activation as a loading control. (E) ER location for Pdi1:GFP and Pdi1$^{\Delta\text{N-gly}}$:GFP. Scale bar represents 10 μm. (F) Indicated strains were spotted onto CM plates supplemented with 2% D-glucose and 4 mM DTT. The mutation of N-glycosylation sites resulted on high DTT sensitivity.

restored the virulence defects observed in $\Delta pdi1$ cells during infection in a similar manner to the *wt* allele, the Pdi1$^{\Delta\text{N-gly}}$ form failed to complement the lack of Pdi1 (Fig 7B) and the Pdi1$^{\Delta\text{N,O-gly}}$ form partially complemented the loss of Pdi1. Similar results were obtained when the different Pdi1 alleles were expressed under the control of the *otef* promoter (S6 Fig). This strongly suggests that only the N-glycosylation of Pdi1 is relevant for its role in virulence. Similarly to $\Delta pdi1$ cells, the virulence defects observed in Pdi1$^{\Delta\text{N-gly}}$, are due to a failure in the fungal expansion inside the plant tissues (Fig 7C). Remarkably, Pdi1$^{\Delta\text{N-gly}}$ could be detected by western blot discarding a possible degradation of Pdi1 in the absence of proper N-glycosylation (Fig 7D). Moreover, Pdi1$^{\Delta\text{N-gly}}$:GFP maintained wild-type Pdi1:GFP subcellular localization to cells membranes and the ER (Fig 7E). Consistent with defective Pdi1 function during plant infection when N-glycosylation target residues are removed, we observed that Pdi1$^{\Delta\text{N-gly}}$ does not complement the DTT sensitivity shown by the Pdi1 deletion mutant (Fig 7F) which has been previously associated to the lack of Pdi1 activity [37].

$\Delta pdi1$ and $\Delta gls1$ show similar secreted protein defects

Taking our results together with the established functions of Pdi1 in other model organisms lead us to propose a model whereby Gls1-mediated glycosylation of Pdi1 is required for correct folding and subsequent secretion of proteins activated by the virulence program. To explore this hypothesis, we compared the secretomes of *wt*, $\Delta pdi1$ and $\Delta gls1$ cells upon Biz1 induction (pathogenic filamentous growth) conditions. We found 6 secreted proteins showing differential electrophoretic mobility in *wt versus* $\Delta pdi1$ cells: UMAG_06158 (probable glutaminase A), UMAG_01829 (Afg1, previously identified in our first screening, see Fig 2), UMAG_04503, an α-N-acetylgalactosaminidase, and UMAG_01213, UMAG_00027 and UMAG_11462 (3 uncharacterized proteins) (see Fig 8). Remarkably, 4 out of these 6 proteins (UMAG_06158, UMAG_01829, UMAG_04503 and UMAG_00027) were also identified in the comparison between *wt* and $\Delta gls1$ secretomes suggesting that the effects caused by $\Delta gls1$ might be explained by deficient Pdi1 function. This indicates that there is a pool of secreted proteins that are glycosylated by Gls1 and their proper folding is dependent on Pdi1, which itself requires Gls1-mediated glycosylation for function. The fact that the number of glycoproteins altered by the loss of *gls1* is higher than by *pdi1* is probably because a group of N-glycoproteins does not require Pdi1 for correct folding, secretion and function (See model Fig 9). This is consistent with the fact that $\Delta gls1$ causes more severe virulence defects than $\Delta pdi1$.

Discussion

In this work, we have demonstrated that the use of glycosylation mutants $\Delta pmt4$ and $\Delta gls1$ in a virulence program-specific 2D-DIGE protein analysis is a suitable and effective approach for
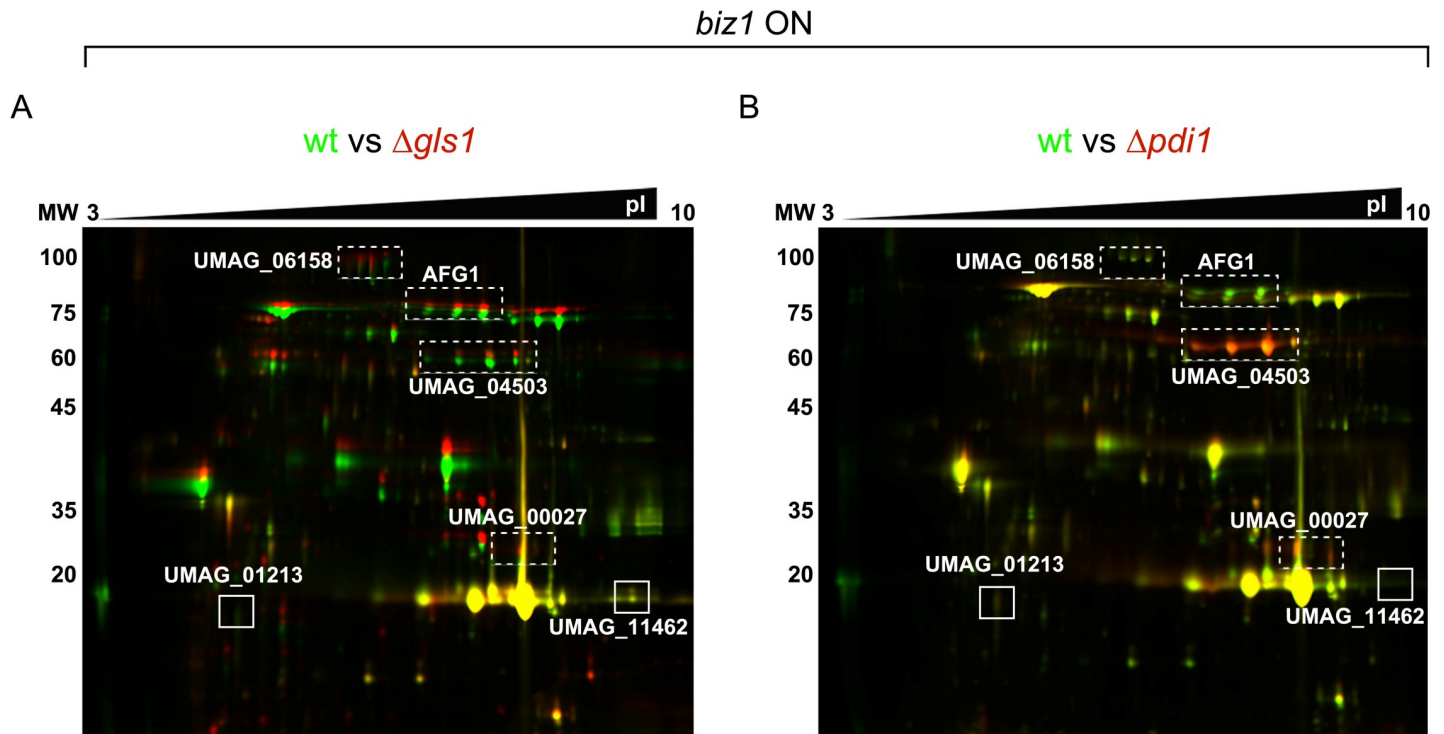
Fig 8. 2D-DIGE expression analysis of Gls1- or Pdi1- dependent secreted glycoproteins. DIGE gel images showing protein changes between wild-type *biz1^crg* (tagged with Cy3 –green) and *gls1* (tagged with Cy5 –red) mutants (A) or between wild-type *biz1^crg* (tagged with Cy3 –green) and *pdi1* (tagged with Cy5 –red) mutants (B). Four glycoproteins depending on both Gls1 and Pdi1 are indicated by dotted rectangles; two additional glycoproteins depending only on Pdi1 are indicated by solid line rectangles.

identifying *Ustilago maydis* glycoproteins involved in plant infection. We identified 35 glycoproteins, and showed that 14 out of the 28 assayed are involved in virulence, analyzing single deletion mutants. Of these mutants, loss of the protein disulfide isomerase Pdi1 had the strongest effect on virulence, most likely due to protein folding defects and changes in functionality and/or secretion of proteins required for plant infection.

An effective method for identifying new glycosylated fungal effectors

It is well established that protein glycosylation is essential for fungal infection. Mutants for specific glycosyltransferases or glycosidases are affected at different stages of the infection process in *Ustilago maydis* [4,5], other plant pathogens such as *Penicilium digitatum* [38], *Magnaporthe oryzae* [15,39] and *Botrytis cinerea* [40] as well as in animal pathogens such as *Candida albicans* [13,41] and *Cryptococcus neoformans* [6,42,43]. Thus, our interest focused on determining which of the glycosylated proteins produced during the infection process were responsible for those defects. We postulated cell wall and secreted proteins as the main sources of novel virulence factors. Cell wall proteins form the pathogen's most external layer while secreted factors have well established roles as effector proteins [44]. Significantly, almost all cell wall and secreted factors are glycosylated [45,46]. *U. maydis* putatively secretes 467 effectors that contribute to the establishment of biotrophy with maize during the infection process [19,22]. *In silico* tools such as SignalP [47], ApoplastP [48] or EffectorP [49] can predict which proteins are secreted and could be putative effectors. Although useful guides, such bioinformatic tools are not completely reliable since it has also been demonstrated that some fungal effectors are not secreted through the canonical secretion pathway involving N-terminal signal
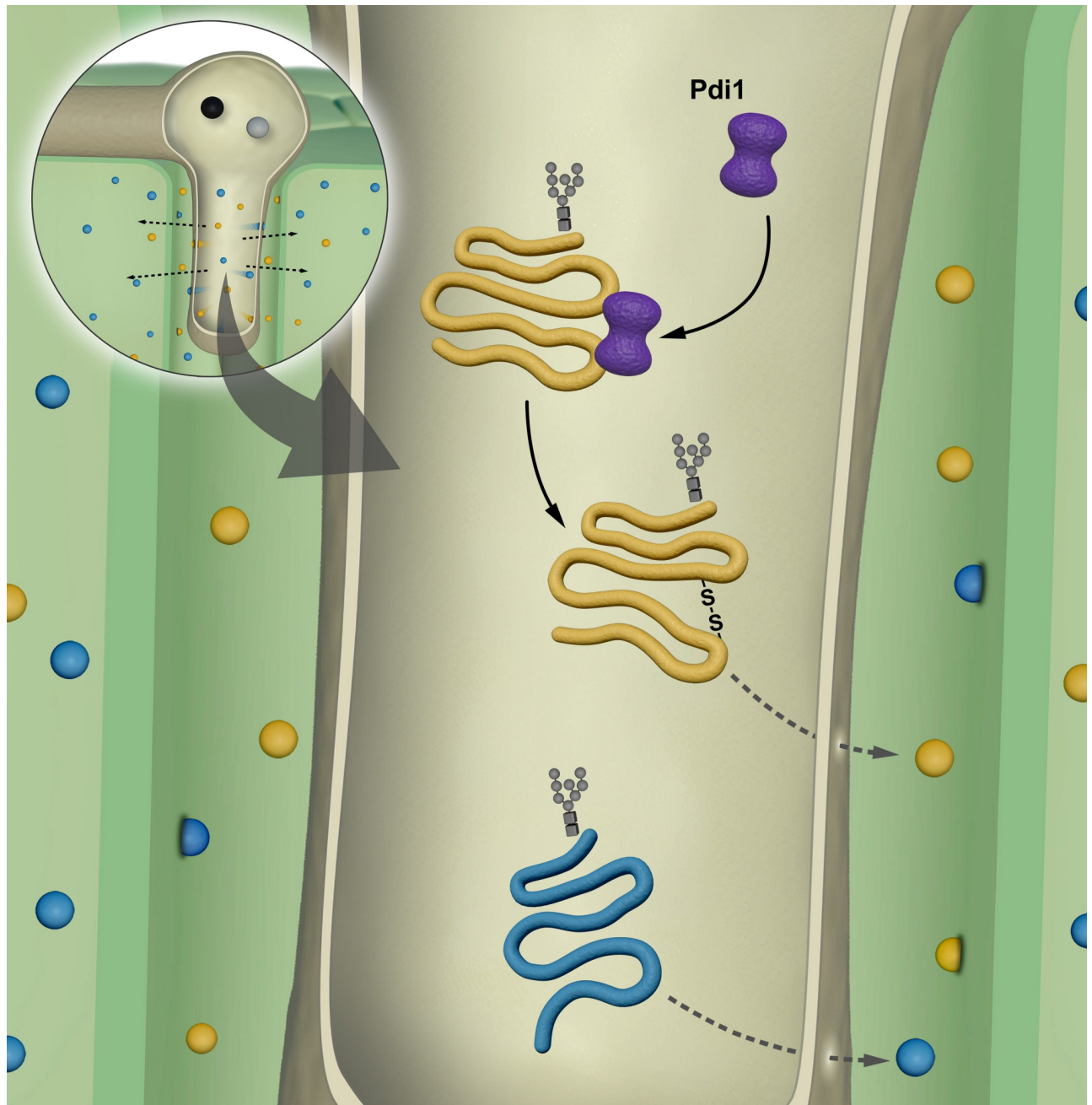
Fig 9. Model of Pdi1 function during infection. Pdi1 assists a subset of glycoprotein in folding and disulfide bonds formation during effector secretion in the apoplast of maize plant during *U. maydis* infection.

peptide degradation prior to translocation to the ER [50–53]. For example, while around 90% of proteins secreted by *Fusarium graminearum* in axenic culture possess a signal peptide, only 56% of proteins secreted during the infection process have secretion signals [54]. Different strategies such as RNA-seq and microarray, have been employed in *U. maydis* in order to identify effectors whose transcription is induced during infection [55–58]. Such studies highlight the huge changes in gene expression that occur during different stages of the infection process. Nevertheless, none of these approaches took into consideration the relevance of protein

modification, which are especially important for secreted proteins. For this reason, a proteomics approach can be an attractive alternative to identify proteins with important roles in the plant infection process. Hence, in this work we established a new strategy to identify glycosylated effectors based on their electrophoretic mobility. Alterations to the glycosylation status of a protein in O- or N-glycosylation mutant strains, Δpmt4 or Δgls1 respectively, can be detected by bidimensional gel electrophoresis. This strategy allowed us to identify 27 glycoproteins from the cytosolic extract, 11 from the secreted protein extract and 6 from the cell wall extract, with some detected in multiple extracts. It is important to highlight that this approach identified previously characterized proteins involved in virulence as well as known effectors such as Afg1 and Afg3 [28], Pep4 [27] and Cmu1 [26]. Among the 35 proteins identified, 4 are cell wall proteins that could be related to plant interaction during infection and 18 are located (Djamei, personal communication) and/or predicted to be located at the apoplastic region (S1 Table), which is consistent with effector protein function. Similar proteomic strategies based on glycosylation changes after the activation of virulence programs have been used to identify new fungal effectors in other pathogenic fungi. For example, the controlled induction of Mst11, a *Magnaporthe oryzae* Mitogen-Activated Protein Kinase (MAPK) essential for appressoria formation and plant infection [59] has been assayed in O-glycosylation mutants such as Δ*MoPmt2* [39] and Δ*MoPmt4* [60], as well as in N-glycosylation mutants such as Δ*alg3* [15] and Δ*Mogls2* [61].

Although it has been described that many single effector gene deletions do not affect plant infection [22], half of the glycoprotein deletions examined in a CL13 background showed a reduction in the number or size of tumors when maize plants were infected (Fig 4 and S2 Fig). In fact, 14 of the 28 single deletion mutants assayed showed a statistically significant decrease in the number of tumors. Interestingly, four of these deletions induced only very small (<1 mm) tumors. Ten of the most promising candidates were then deleted in the SG200 strain and tested for virulence in maize plants, showing that Δ*pdi1* was the least virulent mutant. Single deletions for the other genes in this background caused little or no reduction in virulence. This observation may be explained by the fact that the CL13 strain does not possess the pheromone encoding gene *mfa2* [29] resulting in a reduced ability to develop filaments and produce tumors during maize plant infection. Thus, CL13 is more sensitive to the deletion of genes with minor but important contributions to the infection process.

Total disruption of the whole glycosylation process in *U. maydis* leads to avirulent phenotypes because of its inability to develop functional appressoria (Δ*pmt4*) or due to failure to spread inside the maize plant (Δ*gls1*) [4,5,62], however we did not find a single factor which resembles these phenotypes. The reason why this single factor was not identified might be because *U. maydis* instead uses a pool of glycosylated effectors that work cooperatively to perform the different steps involved in plant invasion and colonization.

Pdi1 is a key factor supporting *U. maydis* pathogenic development

Of all the virulence-related glycoproteins identified here, we chose to further characterize Pdi1 as its deletion led to the strongest reduction in virulence. As we expected, Pdi1 localized to the ER and its deletion led to growth defects in axenic culture when an ER stress-inducing drug such as DTT was added to either solid or liquid media (Fig 5). These results support the idea that Pdi1 is a disulfide-isomerase protein that might assist the folding of newly synthetized proteins in the ER *via* the addition of disulfide bonds, which is critical during ER stress conditions [33]. Hence, the loss of Pdi1 could potentially affect the function of other proteins leading to general defects in different processes such as cell viability, growth, metabolism or cell signaling, among others. Although *pdi1* deletion did not impair cell viability or growth under

normal conditions (S4 Fig), we cannot rule out the possibility that such indirect effects could influence pathogenic progression. Many *U. maydis* effector proteins harbor cysteine-rich regions suitable for the formation of disulfide bonds, which may be necessary for their acquisition of active conformations [22,63,64]. Thus, Pdi1's role in establishing disulfide bonds in proteins involved in plant infection could be a major part of how the Δ*pdi1* mutation affects virulence. Moreover, both calreticulin (CRT) and calnexin (CNX), which bind glycosylated N-glycans in the ER, have a Pro-rich arm that may bind a protein disulfide isomerase [34], such as Pdi1. N-glycans may also play an important role in ER-associated degradation (ERAD) of proteins [34]. Consequently, Pdi1 may be directly or indirectly involved in the selection of mis-folded glycoproteins for dislocation into the cytosol for degradation by proteasomes, i.e., through N-glycans and mannosidase 1 (Mns1) and a second set of proteins called MnlI (man-nosidase-like), Htm1 (homologous to mannosidase), or ER degradation-enhancing α-manno-sidase-like protein (EDEM) [1,34,65,66]. Additionally, it has been shown that Pdi1 from *Botrytis cinerea* is also related to NADPH oxidase signaling [67] and thus Pdi1 could be also involved in ROS production to counteract plant oxidative burst responses.

Modification of the two putative N-glycosylation motifs identified in the Pdi1 ORF affected its ability to recover the infective capacity of a *pdi1* mutant. Because Pdi1 activity, in terms of cell growth capacity under DTT-induced reductive ER stress [37] it suggests that N-glycosyla-tion of Pdi1 may be required for its *in vivo* function. Consistent with this idea, the modification of the putative N-glycosylation motifs affected Pdi1 electrophoretic mobility, without affecting Pdi1 cellular location or stability, making it unlikely that the Pdi1$^{\Delta N\text{-gly}}$ point mutations have grossly affected Pdi1 synthesis or conformation. Moreover, similar alanine substitutions within all nine putative O-glycosylation motifs had no effect on the ability of Pdi1 to rescue the DTT-induced growth defect. Thus, while it remains possible that the two Pdi1$^{\Delta N\text{-gly}}$—point muta-tions have an effect on Pdi1 activity unrelated to N-glycosylation, the most likely explanation of our evidence is that N-glycosylation is specifically required for Pdi1 activity. Interestingly, while the double Pdi1$^{\Delta N,O\text{-gly}}$ mutant shows similar defects in Pdi1 activity as the ΔN- mutant, it actually complements the lack of Pdi1 slightly better than the ΔN- one. In summary, our evi-dence suggests that N-glycosylation of Pdi1 is important for its activity *in vivo* but that further investigation is required to fully understand the role of glycosylation on Pdi1 function.

We have demonstrated that the Pdi1 deletion strain can complete the initial steps of the infection process, appressoria formation and dikaryotic filament formation normally (Fig 6D and 6E). Inside the maize plant, this mutant is able to form clamp-like cells and hyphae spread into maize cells although it cannot reach the vascular tissue. This growth defect was also observed by qPCR fungal biomass quantification, with more than a 50% reduction in fungal biomass versus wild-type (Fig 6G). During *U. maydis* biotrophic development until tumor for-mation at 6 dpi, the fungus has to form the dikaryotic filament, develop appressoria, penetrate into the plant, modify plant metabolism to avoid activation of the plant's immune system and ensure its proper propagation inside the host. In order to achieve all these tasks, *U. maydis* secretes several early effectors such as Pep1 [68,69], Pit2 [70], Stp1 [35] and See1 [71]. As Δ*pdi1* did not show any defects in appressoria formation, dikaryotic filament formation or maize plant penetration, the reduction in fungal biomass observed in this mutant may be the result of a failure of the folding and secretion of proteins to the apoplast. Therefore, we propose four non-mutually exclusive mechanisms by which the loss of Pdi1 could affect fungal viru-lence: i) a reduction in ER stress resistance and defective Reactive Oxygen Species (ROS) sig-naling; ii) a decrease or abolition in the secretion of effectors; iii) a reduction or elimination of the activity of the secreted effectors; iv) the presence of abnormally folded proteins that behave as new pathogen-associated molecular patterns (PAMPs) and activate the plant immune sys-tem. Work towards deciphering the molecular basis of Pdi1 action during plant infection and

testing the above hypotheses is currently ongoing in our laboratory. Our results raise the possibility that mechanisms linking glycosylation and disulfide bond formation of fungal effectors are conserved and highlight the need to explore Pdi1's role in other fungal pathogens.

Materials and methods

Strains, plasmid and growth conditions

Escherichia coli DH5α and pGEM-T easy (Promega) and pJET1.2/blunt (ThermoFisher Scientific) were used for cloning purposes. Growth conditions for *E. coli* [72] and *U. maydis* [73] have been previously described. *U. maydis* strains used in this study are listed in S2 Table.

To induce the over-expression of transcription factor Biz1 [24], FB1Biz1^{crg} and its derivative mutants (FB1Biz1^{crg}Δ*pmt4*, FB1Biz1^{crg}Δ*gls1* and FB1Biz1^{crg}Δ*pdi1*) cells were grown at 28ºC in complete medium (CM) supplemented with D-glucose 25% (CMD), washed twice with water and grown in CM supplemented with arabinose 25% (CMA) at 28ºC for 8 hours.

Pathogenicity assays were performed as described in [19]. *U. maydis* cultures were grown at 28ºC to exponential phase in liquid YEPSL (0.4% bactopeptone, 1% yeast extract and 0.4% saccharose) and concentrated to an OD$_{600}$ of 3, washed twice in water and injected into 7 days old maize (*Zea mays*) seedlings (Early Golden Bantam). Disease symptoms were quantified 14 dpi. Statistical analyses were performed in GraphPad Prism 6 software.

ER stress assays were carried out with cultures grown at 28ºC to exponential phase in CMD and spotted at 0.4 OD$_{600}$ onto CM plates supplemented with 4 mM DTT (iNtRON Biotechnology). Plates were incubated for 48 h at 28ºC. For ER stress assay in liquid culture, *U. maydis* cells were grown to exponential phase in YEPSL and diluted to 0.1 OD$_{600}$ in YEPSL with 10 mM DTT. Cell growth at 28ºC with continuous shaking was analyzed over 24 h using a Spark 10M (Tecan) fluorescence microplate reader.

Cell wall integrity and oxidative stress assays were carried out with cultures grown at 28ºC to exponential phase in CMD and spotted at 0.4 OD$_{600}$ in CM plates supplemented with calcofluor white 40 μg/ml (Sigma-Aldrich), Congo Red 50 μg/ml (Sigma-Aldrich), Tunicamycin 1 μg/ml (Sigma-Aldrich), Sorbitol 1M (Sigma-Aldrich), 2% DMSO (Sigma-Aldrich), H$_2$O$_2$ 1.5 mM (Sigma-Aldrich) and NaCl 1M (Sigma-Aldrich). Plates were incubated for 48 h at 28ºC.

For mating and filamentation assays, cells were grown in liquid YEPSL until exponential phase, washed twice with sterile bidistilled water, spotted onto PD-charcoal plates and grown for 24–48 hours at 25-28ºC.

DNA and RNA procedures

Molecular biology techniques were used as described in [72]. *U. maydis* DNA isolation and transformation were carried out following the protocol described in [74].

To generate deletion mutants, 1 kb fragments of the 5' and 3' flanks of the gene of interest (*goi*) ORF were generated by PCR using Phusion High Fidelity DNA polymerase (New England Biolabs) or Q5 High-Fidelity DNA polymerase (New England Biolabs) and *U. maydis* FB1 genomic DNA, using the primers *goi*KO5-1 and *goi*KO5-2 (containing a *Sfi*I restriction site) to amplify the 5' flank and *goi*KO3-1 (containing a *Sfi*I restriction site) and *goi*KO3-2 to amplify the 3' flank (S3 Table). These fragments were digested with *Sfi*I and ligated with the 1.9-kb *Sfi*I carboxin, 1.4-kb *Sfi*I noursethricin (*ClonNAT*), 2-kb *Sfi*I geneticin or 1.9-kb *Sfi*I hygromicin resistance cassettes [75]. Constructs were cloned into pGEM-T easy (Promega) or pJET1.2/blunt (ThermoFisher Scientific) plasmids and amplified by PCR using the primers *goi*KO5-1/*goi*KO3-2, prior to their transformation in *U. maydis*.

To generate SG200 2xRFPΔ*pdi1* used for filament quantification into the maize plant, pGEM-TΔ*pdi1*:*cbx* plasmid was digested with *Sfi*I to excise the carboxin resistance cassette

and ligated to a hygromicin resistance cassette isolated from pMF1h [75] with *Sfi*I/*Bsa*I double digestion, leading to pGEM-TΔ*pdi1:hyg*. This construct was amplified by PCR with Phusion DNA polymerase using primers pdi1KO5-1/pdi1KO3-2 and integrated into the SG200 2xRFP strain [76].

For the SG200 3xGFP strain used for filament quantification *in planta*, the pOG plasmid [76], containing 3xGFP under the control of the *otef* promotor and a hygromicin resistance cassette, was digested with *Psi*I and integrated into the SG200 strain. Finally, Δ*pdi1:cbx* was amplified by PCR using primers pdi1KO5-1/pdi1KO3-2 and integrated into the SG200 3xGFP strain.

To perform *pdi1* deletion complementation assays, we generated the SG200Δ*pdi1*P$_{otef}$*pdi1* strain. To this end, the eGFP fragment in p123 [77] was substituted with the *pdi1* ORF. The *pdi1* ORF was amplified by PCR using Phusion HF DNA polymerase (New England Biolabs) with primers pdi1StartXmaI and pdi1StopNotI, containing *Xma*I and *Not*I restriction sites, respectively. The PCR product was digested with *Xma*I and *Not*I, purified and cloned into the p123 plasmid digested with both restriction enzymes, creating p123-*pdi1*. Finally, p123-*pdi1* was linearized with *Ssp*I and integrated into the SG200Δ*pdi1 ip* locus by homologous recombination.

To create an O-glycosylation deficient *pdi1* mutant, serine or threonine sites predicted by NetOgly 4.0 tool were replaced by site-direct mutagenesis using GenScript (Piscataway, USA), generating the plasmid pUC57-*pdi1*mutO-gly, with *Sma1* and *Not*I restriction sites. The *pdi1*-mutO-gly construct was reintroduced into p123 as described above, creating the p123-*pdi1*-mutO-gly vector. This plasmid was linearized with *Ssp*I and integrated into the SG200Δ*pdi1 ip* locus by homologous recombination, generating the SG200Δ*pdi1pdi*$^{ΔO-gly}$ strain.

To generate an N-glycosylation mutant version of *pdi1*, asparagine 36 and 484 were replaced by glutamine in N-glycosylation sites through PCR using the Gibson Assembly Cloning Kit (New England BioLabs, Frankfurt, Germany) with primers PDI1Asn36mut-1 and PDI1Asn36mut-2 for the mutation N36Q and primers PDI1Asn484mut-1 and PDI1Asn484-mut-2 for the mutation N484Q, using p123-*pdi1* as template, generating the plasmid p123-*pdi1*mutN-gly. This construction was integrated into the SG200Δ*pdi1 ip* locus (as described above), leading to SG200Δ*pdi1pdi*$^{ΔN-gly}$ strain.

To generate the O- and N-glycosylation *pdi1* mutant, N36 and N484 was replaced by glutamine using PCR and the Gibson Assembly Cloning Kit, with primers PDI1Asn36mut-1/PDI1Asn36mut-2 for the N36Q mutation and PDI1Asn484mutThr486mut-1/PDI1Asn484-mutThr486mut-2 for the N484Q mutation, and the plasmid p123-*pdi1*mutO-gly as template, reintroduced into p123 to generate p123-*pdi1*mutN,O-gly. This construct was linearized with *Ssp*I and reintegrated into the SG200Δ*pdi1 ip* locus.

All *pdi1* mutants for N- and/or O-glycosylation were confirmed by sequencing, using primers PDI1SeqI and PDI1SeqII.

To generate plasmids containing the different *pdi1* versions under the control of the *pdi1* promoter, plasmids p123-*pdi1*, p123-*pdi1*mutN-gly, p123-*pdi1*mutO-gly and p123-*pdi1*mutN,O-gly were digested with *Pvu*II and *Sma*I restriction enzymes to eliminate the *otef* promoter and purified. The *pdi1* promoter was then amplified by PCR using Q5 DNA polymerase with primers pPdi1-F-NEB and pPdi1-R-NEB containing a p123 plasmid overlapping sequence of 20 bp and cloned into the different p123 derivative plasmids with NEBuilder HiFi DNA Assembly (New England Biolabs), according to the manufacturer's protocol. These vectors were linearized with *Ssp*I and reintegrated into the SG200Δ*pdi1 ip* locus by homologous recombination, leading to SG200Δ*pdi1* pPdi1:*pdi1*^{wt}, SG200Δ*pdi1* pPdi1:*pdi*$^{ΔO-gly}$, SG200Δ*pdi1* pPdi1:*pdi*$^{ΔN-gly}$ and SG200Δ*pdi1* pPdi1:*pdi*$^{ΔN,O-gly}$ strains.

For GFP tagging of *pdi1*, we generated plasmid pDL51-*pdi1*. This plasmid is a p123 derivative [16] where *pdi1* ORFs were PCR amplified using Phusion DNA polymerase with primers pdi1ORF5/pdi1ORF3, was cloned in frame with the GFP present in the plasmid, under the

control of the constitutive expressed *otef* promotor. To achieve this, pDL51 was linearized with *Sfi*I digestion and ligated with the *pdi1* ORF digested with *Sfi*I. For GFP tagging of the N-glycosylation mutant version of Pdi, *pdi1*mutN-gly was amplified by PCR with primers pdi1StartXmaI and pdi1Stop*Nco*I containing *Xma*I and *Nco*I restriction sites, respectively. The PCR product was digested with *Xma*I and *Nco*I, purified and cloned into the p123GFP plasmid digested with both restriction enzymes, to generate an in frame C-terminal *pdi1*mutN-gly GFP fusion. Finally, p123-*pdi1*mutN-glyGFP was linearized with *Ssp*I and integrated into the SG200Δ*pdi1 ip* locus by homologous recombination.

For fungal biomass quantification, 3 and 5 dpi maize leaves were grown in liquid nitrogen and total DNA was isolated with DNeasy Plant Mini kit (Qiagen) according to manufacturer's instructions. Fungal biomass was then quantified by Real-Time PCR with an ABIPRISM 7000 Sequence Detection System (Applied Biosystems) using the Power SYBR Green PCR Master Mix (ThermoFisher Scientific) according to the manufacturer's protocol, measuring the constitutively-expressed fungal *ppi1* gene, using primers RT-PPI1-5/RT-PPI1-3, and and constitutively-expressed plant *gapdh*, using primers Gapdh-F/Gapdh-R for normalization purposes. 100 ng of total DNA was used a template for each reaction.

For Pdi1 expression analysis, RNA from FB1 axenic culture and maize plants infected with FB1 and FB2 was isolated at 1, 3, 5 and 9 dpi, ground in liquid nitrogen using a pestle and mortar and purified using TRIzol reagent (Thermo Fisher Scientific) and the Direct-zol RNA Miniprep Plus kit (Zymo Research), following the manufacturer's instructions. cDNA was synthetized using RevertAid H Minus First Strand cDNA Synthesis kit (Thermo Fisher Scientific) following the manufacturer's instructions. Pdi1 expression levels were quantified by qRT-PCR using a Real-Time CFX Connect (Biorad) and SYBR Premix Ex Taq II (Tli RNase H Plus) (Takara) according to the manufacturer's protocol, measuring *pdi1* expression gene, using primers pdi1 RT-fwd/pdi1 RT-rev, and *ppi1* as a constitutively-expressed control, using primers RT-PPI1-5/RT-PPI1-3.

Proteomic analysis

To detect pathogenesis-related changes to the cytosolic proteome caused by the loss of *pmt4*, we isolated O-glycosylated proteins from FB1Biz1*crg* and FB1Biz1*crg*Δ*pmt4* strains. FB1 and FB1Δ*pmt4* strains were used as controls. Cells from each strain were grown in 1 L of CMD to an $OD_{600} = 0.5$–0.8, washed twice with sterile bidistilled water and grown for 8 hours in 1 L of CMA. After filamentation induction, samples were harvested by centrifugation, washed twice in ice-cold 20 mM Tris-HCl buffer (pH 8.8) and frozen at −80ºC. Cells were then resuspended in lysis buffer (20 mM Tris-HCl, 0.5 M NaCl, pH 7.4) containing protease inhibitor cocktail (cOmplete Tablets, EDTA-free, Roche) after which cell lysis was performed using glass beads (Sigma) in a FastPrep-24 homogeniser (MP Biomedicals), with power set to 6.0 using 3 x 45" pulses at maximum speed with 5 min rest between cycles. After cell lysis, tubes were drilled with a needle and put into a new tube and samples were recovered by centrifugation at 4000 rpm for 1 min. Subsequently, samples were centrifuged at 14000 rpm for 30 min at 4ºC and the supernatant was collected. One volume of 2x binding buffer (20 mM Tris-HCl, 0.5 M NaCl, 2 mM $MnCl_2$, 2 mM $CaCl_2$, pH 7.4) was added and concentrated using Amicon Ultra-15 3 kDa centricon (Merk Millipore) and O-glycosylated proteins isolated by affinity chromatography using Concavaline A columns (HiTrap Con A 4B, GE Healthcare) in AKTA FPLC (GE Healthcare), and eluted with a buffer containing 20 mM Tris-HCl, 0.5 M NaCl and 0.5 M methyl-α-D-manopyranoside (pH 7.4).

To detect pathogenesis-related changes to the cytosolic proteome caused by the loss of *gls1*, FB1Biz1*crg* and FB1Biz1*crg*Δ*gls1* cells were grown in 1 L of CMD to an $OD_{600} = 0.5$–0.8, washed

twice with sterile distilled water and grown for 8 hours in 1 L of CMA. FB1 and FB1Δ*gls1*, used as controls, were grown in 2 L of CMD to an OD_{600} = 0.5–0.8, washed twice with sterile distilled water and grown during 8 hours in 2 L of CMA. Samples were harvested by centrifugation, washed twice in ice-cold 20 mM Tris-HCl buffer (pH 8.8) and frozen by dropping samples in liquid nitrogen. Cells were lysed with 3–4 cycles in 6870 Freezer/Mill (SPEX, SamplePrep) according to the manufacturer's instructions. Samples were resuspended in binding buffer (20 mM Tris-HCl, 0.5 M NaCl, 2 mM $MnCl_2$, 2 mM $CaCl_2$, pH 7.4) containing protease inhibitor cocktail (cOmplete Tablets, EDTA-free, Roche) and centrifuged at 14000 rpm for 30 min at 4ºC. Supernatant was filtered and N-glycosylated proteins isolated by affinity chromatography using Concavaline A columns (HiTrap Con A 4B, GE Healthcare) in AKTA FPLC (GE Healthcare), and eluted with a buffer containing 20 mM Tris-HCl, 0.5 M NaCl and 0.5 M methyl-α-O-glucopyranoside (pH 7.4).

For differential analysis of secreted O- or N-glycoproteins in Δ*pmt4* or Δ*gls1* mutants, FB1Biz1^{crg} and FB1Biz1^{crg}Δ*pmt4* or FB1Biz1^{crg}Δ*gls1* cells were grown in 1 L of CMD to an OD_{600} = 0.5–0.8, washed twice with sterile bidistilled water and grown for 8 hours in 1 L of CMA. After filamentation induction, cells were centrifuged, the supernatant filtered and secreted glycosylated proteins precipitated with deoxycholate acid and TCA.

Cell wall O- or N-glycoproteins in Δ*pmt4* or Δ*gls1* mutants were purified following the protocol described in [78], with some modifications. FB1Biz1^{crg} and FB1Biz1^{crg}Δ*pmt4* or FB1Biz1^{crg}Δ*gls1* cells were grown in 1 L of CMD to an OD_{600} = 0.5–0.8, washed twice with sterile bidistilled water and grown for 8 hours in 1 L of CMA. After filamentation induction, samples were harvested by centrifugation, washed four times in ice-cold 10 mM Tris-HCl buffer (pH 7.4) and frozen at −80ºC. Cells were then resuspended in 10 mM Tris-HCl buffer (pH 7.4) containing protease inhibitor cocktail (cOmplete Tablets, EDTA-free, Roche) after which cell lysis was performed with glass beads (Sigma) in a FastPrep-24 homogeniser (MP Biomedicals), with power set to 6.5 using 6 x 60" pulses at maximum speed with 3 minutes rest between cycles. Samples were recovered by centrifugation at 3000 x g for 10 min at 4ºC, after drilling the bottom of the tube with a needle and placing into a new tube. The pellet (cell wall) was collected and washed sequentially with ice-cold sterile bidistilled water, 5% NaCl with protease inhibitor, 2% NaCl with protease inhibitor and 1% NaCl with protease inhibitor. Washing steps were repeated three more times and cell wall proteins (CWPs) purified after 10 min at 100ºC in extraction buffer (50 mM Tris-HCl pH 8.0, 100 mM EDTA, 2% SDS, 10 mM DTT) followed by 15 min centrifugation at 35000 x g. CWPs were then collected from the supernatant.

To analyze the common target between Gls1 and Pdi1, secreted proteins from FB1Biz1^{crg} and FB1Biz1^{crg}Δ*gls1* or FB1Biz1^{crg}Δ*pdi1* were precipitated with deoxycholate acid and trichloroacetic acid (TCA) following the protocol described above for secreted O- and N-glycoproteins.

Isolated proteins for each fraction and genotype were then precipitated with 2D Clean-Up kit (GE Healthcare), and dissolved in TS buffer (7M urea, 2M thiourea, and 4% CHAPS) containing 30 mM Tris-HCl (pH 9.5). Protein concentration was determined using RC DC Protein Assay (Bio-Rad).

Fifty micrograms of protein extract from each sample were labeled with Cy3- or Cy5 Dye (GE Healthcare). Labeling was performed reciprocally so that each sample was separately labeled with Cy3 and Cy5 to account for any preferential protein labeling by the CyDyes. Twenty-five micrograms of each sample were labeled with Cy2-Dye and pooled together as an internal standard. Labeling was performed according to the manufacturer's instructions. Different Isoelectric Focusing (IEF) procedures were performed. For cytosolic O-glycoproteins and CWPs, IEF was performed in 24 cm 4–7 NL Immobiline DryStrip (GE Healthcare) in an

IPGphor unit (GE Healthcare) at 20ºC as follows: rehydratation for 12 h, 500 V for 1 h, linear gradient from 500 to 1000 V for 1 h, linear gradient from 1000 to 8000 V for 3 h and 8000 V to 60000 total Vhr for 5.5 h. The same IEF procedure using 24 cm 3–10 NL DryStrips was performed for secreted proteins. For cytosolic N-glycoproteins, IEF was performed using 24 cm 3–7 NL Immobiline DryStrip (GE Healthcare) in an IPGphor unit (GE Healthcare) at 20ºC as follows: rehydration for 12 h, 500 V for 1.5 h, linear gradient from 500 to 1000 V for 7 h, linear gradient from 1000 to 8000 V for 8 h and 8000 V to 60000 total Vhr for 5.5 h. After IEF, strips were incubated for 15 min at room temperature in a shaker in equilibration buffer (50 mM Tris-HCl [pH 8.5], glycerol 30% v/v, 6M urea, 2% w/v SDS) with 10 mg/mL DTT, followed by another 15 min incubation in equilibration buffer with 25 mg/mL iodoacetamide and loaded onto 10% acrylamide gels. Second dimension separation was performed using an EttanDalt Six Electrophoresis Unit (GE Healthcare).

After electrophoresis, gels were imaged using a Typhoon-9400 scanner (GE Healthcare) with a 100 μm resolution using appropriate emission and excitation wavelengths, photomultiplier sensitivity and filters for each of the Cy2, Cy3, and Cy5 dyes.

Relative protein spot quantification across experimental conditions was performed automatically and in a blind manner using DeCyder v7.0 software and the multivariate statistical module EDA v7.0 (Extended Data Analysis, GE Healthcare) as follows. First, the Batch Processor module detected spots across the three gel images (two experimental samples and an internal standard) and generates differential in-gel analysis images with information about spot abundance in each image with values expressed as ratios. After spot detection, the biological variation analysis module utilizes differential in-gel analysis images to match protein spots across all gels, using the internal standard for gel-to-gel matching. Statistical analysis was then carried out to determine protein expression changes. To perform a restrictive analysis, we considered spot changes significant when associated with a p-value lower than 0.01. This value was chosen based on Student's t-test with multiple testing assessed using the false discovery rate. Multivariate analysis was performed by principal component analysis using the algorithm included in the DeCyder EDA module based on spots matched across all gels.

Protein identification was performed at the Proteomics Unit of the Pablo de Olavide University (Seville, Spain) and at the Proteomics service of Parque Científico de Madrid (Madrid, Spain). Spots were excised from the gels manually and transferred to 1.5 mL tubes. Sample digestion and MALDI-MS and MS/MS database searches were done by the Proteomics Units mentioned above.

Western blot analyses

For Western Blot analyses, cells were grown in YEPSL to an OD_{600} = 0.6–0.8 and were then collected by centrifugation at 4500 rpm for 5 min, washed twice with 20 mM Tris-HCl pH 8.8 and pellets were resuspended in lysis buffer (20 mM Tris-HCl, 0.5 M NaCL, pH 7.4) with protease inhibitor cocktail (cOmplete Tablets, EDTA-free, Roche). Samples lysis was performed with glass beads (Sigma) in a FastPrep-24 homogeniser (MP Biomedicals), with power set to 6.5 using 6 x 60" pulses at maximum speed with 4 minutes rest between cycles. After cell lysis, tubes were drilled with a needle and put into a new tube and samples were recovered by centrifugation at 4000 rpm for 1 min. Subsequently, samples were centrifuged at 14000 rpm for 30 min at 4ºC and the supernatant was collected. Protein concentration was measured using the RC DC Protein Assay kit (Bio-Rad). 60 μg of protein extract for each strain analyzed was loaded into a 10% TGX Stain-Free FastCast Acrylamide gel (Bio-Rad). Separated proteins were transferred onto a nitrocellulose membrane using the Trans-Blot Turbo transfer system (Bio-Rad). The membrane was incubated with mouse polyclonal anti-GFP antibody (Roche)

(1:1000). As secondary antibody, anti-mouse IgG-horseradish peroxidase conjugated antibody (1:5000; Sigma Aldrich) was used. Immunoreactive bands were developed by SuperSignal West Femto Maximum Sensitivity substrate (ThermoFisher Scientific). Image gel and membrane acquisition was carried out with ChemiDoc XRS (Bio-Rad).

Microscopy

To corroborate ER Pdi1 localization, experimental SG200*pdi1*:*gfp* and ER localization control SG200*cal^s*:*mrfp*:*HDEL* cells [79] were visualized using a spinning-disk confocal microscope (IX-81, Olympus; CoolSNAP HQ2 camera, Plan Apochromat 100×, 1.4 NA objective, Roper Scientific). To determine ER Pdi1$^{\Delta N\text{-}gly}$:GFP localization, SG200*pdi1$^{\Delta N\text{-}gly}$*:*gfp* and SG200*pdi1*: *gfp* cells were visualized using a DeltaVision microscopy system comprising an Olympus IX71 microscope and CoolSnap HQ camera.

For morphology visualization, cells were observed by Differential Interference Contrast (DIC) using a DeltaVision microscopy system comprising an Olympus IX71 microscope and CoolSnap HQ camera.

For *in planta* quantification of filament and appressoria formation in co-infection experiments with *U. maydis* GFP and RFP labeled strains, 15 dpi leaf samples were stained with calcofluor white (Sigma-Aldrich) to visualize fungal material and then checked for GFP or RFP fluorescence.

To analyze the *U. maydis* progression inside the maize plant, leaf samples from 3 and 5 dpi infected plants were distained with ethanol, treated 4h at 60ºC with 10% KOH, washed in phosphate buffer and then stained with propidium iodide (PI) to visualize plant tissues in red and wheat germ agglutinin (WGA)/AF488 to visualize the fungus in green. Samples were examined using a Leica SPE (DM2500) confocal microscope. Image processing was carried out using Adobe Photoshop CS5 and ImageJ.

Supporting information

S1 Fig. Script for O- and N-glycosylation site identification.
(DOCX)

S2 Fig. Individual infection assays of pathogenic pathway glycoprotein candidates. Deletions and infections were first carried out in the CL13 strain (A). Deletions showing a statistically significant reduction in virulence were then assayed in SG200 (B) and subsequently in FB1 and FB2 compatible strains (C). Total number of plants infected is indicated above each column. The Mann-Whitney statistical test was performed (ns: not statistically significant; * for p-value < 0.05; ** for p-value < 0.01; *** for p-value < 0.005; **** for p-value < 0.0001).
(TIF)

S3 Fig. UMAG_10156 is similar to *Saccharomyces cerevisiae* Pdi1. Alignment of Pdi1 sequence from *S. cerevisiae* and UMAG_10156 from *U. maydis* using T-Coffee Server and Box-Shade Server. Thioredoxin domains are indicated by red lines.
(TIF)

S4 Fig. Loss of *pdi1* has no effect on the non-pathogenic stage. (A) Growth rate of SG200 and SG200 Δ*pdi1* in liquid rich media YEPSL. (B) SG200 and Δ*pdi1* cells observed by DIC microscopy do not show any defect in size and morphology.
(TIF)

S5 Fig. N-glycosylation mutation in Pdi1 does not affect cell wall integrity nor oxidative stress. Osmotic (1) and oxidative (2) stress, cell wall integrity (3) and ER stress (4) assays were

performed in CM plates supplemented with 2% D-glucose and Sorbitol 1M, NaCl 1M, H_2O_2 1.5 mM, calcofluor white (CFW) 40 μg/ml, Congo Red 50 μg/ml, Tunicamycin 1 μg/ml and 2% DMSO as Tunicamycin solvent control.
(TIF)

S6 Fig. Pdi1$^{ΔN\text{-}gly}$ allele expressed under the control of the otef promoter failed to complement the lack of Pdi1. The percentage of symptoms in maize plants infected with the indicated strains at 14 dpi. The total number of infected plants is indicated above each column. Mann-Whitney statistical test was performed (ns: not statistically significant; *** for *p*-value < 0.005).
(TIF)

S1 Table. Identified glycoproteins in this study. List of glycoproteins identified through the three different extracts indicating in which extract were identified, their apoplastic secretion prediction and their gene deletion phenotypes after maize plant infection.
(XLSX)

S2 Table. List of strains used in this study.
(DOCX)

S3 Table. List of primers used in this study.
(DOCX)

S4 Table. Mann-Whitney statistical test individually performed for each pathogenic assay in Fig 7B. The Mann-Whitney statistical test was applied to each strain versus Δ*pdi1* and Δ*pdi1* pPdi1:pdi1 (pdi1^{wt}) for each independent experiment (R1, R2 and R3). *P*-values obtained are listed in this table. Statistical significance is indicated by *p*-values in bold.
(DOCX)

Acknowledgments

Author Contributions

Conceptualization: Ismael Moreno-Sánchez, Ramón R. Barrales, Alfonso Fernández-Álvarez, José Ignacio Ibeas.

Data curation: Alfonso Fernández-Álvarez, José Ignacio Ibeas.

Formal analysis: Miriam Marín-Menguiano, Ismael Moreno-Sánchez, Alfonso Fernández-Álvarez, José Ignacio Ibeas.

Funding acquisition: José Ignacio Ibeas.

Investigation: Miriam Marín-Menguiano, Ismael Moreno-Sánchez, Ramón R. Barrales, José Ignacio Ibeas.

Methodology: Miriam Marín-Menguiano, Ismael Moreno-Sánchez, Ramón R. Barrales, Alfonso Fernández-Álvarez, José Ignacio Ibeas.

Project administration: José Ignacio Ibeas.

Resources: José Ignacio Ibeas.

Supervision: Ramón R. Barrales, Alfonso Fernández-Álvarez, José Ignacio Ibeas.

Validation: Alfonso Fernández-Álvarez, José Ignacio Ibeas.

Writing – original draft: Ismael Moreno-Sánchez, Alfonso Fernández-Álvarez, José Ignacio Ibeas.

Writing – review & editing: Miriam Marín-Menguiano, Ismael Moreno-Sánchez, Ramón R. Barrales, Alfonso Fernández-Álvarez, José Ignacio Ibeas.

References

1. Helenius A, Aebi M. Roles of N-Linked Glycans in the Endoplasmic Reticulum. Annu Rev Biochem. Annual Reviews 4139 El Camino Way, P.O. Box 10139, Palo Alto, CA 94303–0139, USA; 2004; 73: 1019–1049. https://doi.org/10.1146/annurev.biochem.73.011303.073752 PMID: 15189166

2. Corfield AP, Berry M. Glycan variation and evolution in the eukaryotes. Trends Biochem Sci. 2015; 40: 351–359. https://doi.org/10.1016/j.tibs.2015.04.004 PMID: 26002999

3. Freeze HH, Eklund EA, Ng BG, Patterson MC. Neurological Aspects of Human Glycosylation Disorders. Annu Rev Neurosci. 2015; 38: 105–125. https://doi.org/10.1146/annurev-neuro-071714-034019 PMID: 25840006

4. Fernandez-Alvarez A, Elias-Villalobos A, Ibeas JI. The O-mannosyltransferase PMT4 is essential for normal appressorium formation and penetration in Ustilago maydis. Plant Cell. 2009; 21: 3397–3412. https://doi.org/10.1105/tpc.109.065839 PMID: 19880800

5. Fernandez-Alvarez A, Elias-Villalobos A, Jimenez-Martin A, Marin-Menguiano M, Ibeas JI. Endoplasmic reticulum glucosidases and protein quality control factors cooperate to establish biotrophy in Ustilago maydis. Plant Cell. 2013; 25: 4676–4690. https://doi.org/10.1105/tpc.113.115691 PMID: 24280385

6. Olson GM, Fox DS, Wang P, Alspaugh JA, Buchanan KL. Role of protein O-mannosyltransferase Pmt4 in the morphogenesis and virulence of Cryptococcus neoformans. Eukaryot Cell. 2007; 6: 222–34. https://doi.org/10.1128/EC.00182-06 PMID: 17142566

7. Rouabhia M, Schaller M, Corbucci C, Vecchiarelli A, Prill SK-H, Giasson L, et al. Virulence of the fungal pathogen Candida albicans requires the five isoforms of protein mannosyltransferases. Infect Immun. 2005; 73: 4571–80. https://doi.org/10.1128/IAI.73.8.4571-4580.2005 PMID: 16040968

8. Schirawski J, Bohnert HU, Steinberg G, Snetselaar K, Adamikowa L, Kahmann R. Endoplasmic Reticulum Glucosidase II Is Required for Pathogenicity of Ustilago maydis. Plant Cell. 2005; 17: 3532–3543. https://doi.org/10.1105/tpc.105.036285 PMID: 16272431

9. Schwarz F, Aebi M. Mechanisms and principles of N-linked protein glycosylation. Curr Opin Struct Biol. 2011; 21: 576–582. https://doi.org/10.1016/j.sbi.2011.08.005 PMID: 21978957

10. Breitling J, Aebi M. N-linked protein glycosylation in the endoplasmic reticulum. Cold Spring Harb Perspect Biol. 2013; 5: a013359. https://doi.org/10.1101/cshperspect.a013359 PMID: 23751184

11. Loibl M, Strahl S. Protein O-mannosylation: What we have learned from baker's yeast. Biochim Biophys Acta—Mol Cell Res. 2013; 1833: 2438–2446. https://doi.org/10.1016/j.bbamcr.2013.02.008 PMID: 23434682

12. Fabre E, Hurtaux T, Fradin C. Mannosylation of fungal glycoconjugates in the Golgi apparatus. Curr Opin Microbiol. 2014; 20: 103–10. https://doi.org/10.1016/j.mib.2014.05.008 PMID: 24934559

13. Hall RA, Gow NAR. Mannosylation in Candida albicans: role in cell wall function and immune recognition. Mol Microbiol. 2013; 90: 1147–1161. https://doi.org/10.1111/mmi.12426 PMID: 24125554

14. Oka T, Hamaguchi T, Sameshima Y, Goto M, Furukawa K. Molecular characterization of protein O-mannosyltransferase and its involvement in cell-wall synthesis in Aspergillus nidulans. Microbiology. 2004; 150: 1973–1982. https://doi.org/10.1099/mic.0.27005-0 PMID: 15184583

15. Chen X-L, Shi T, Yang J, Shi W, Gao X, Chen D, et al. N-Glycosylation of Effector Proteins by an α-1,3-Mannosyltransferase Is Required for the Rice Blast Fungus to Evade Host Innate Immunity. Plant Cell. 2014; 26: 1360–1376. https://doi.org/10.1105/tpc.114.123588 PMID: 24642938

16. Fernandez-Alvarez A, Marin-Menguiano M, Lanver D, Jimenez-Martin A, Elias-Villalobos A, Perez-Pulido AJ, et al. Identification of O-mannosylated virulence factors in Ustilago maydis. PLoS Pathog. 2012; 8: e1002563. https://doi.org/10.1371/journal.ppat.1002563 PMID: 22416226

17. Kamper J, Reichmann M, Romeis T, Bolker M, Kahmann R. Multiallelic recognition: nonself-dependent dimerization of the bE and bW homeodomain proteins in Ustilago maydis. Cell. 1995; 81: 73–83. https://doi.org/10.1016/0092-8674(95)90372-0 PMID: 7720075

18. Mendoza-Mendoza A, Berndt P, Djamei A, Weise C, Linne U, Marahiel M, et al. Physical-chemical plant-derived signals induce differentiation in Ustilago maydis. Mol Microbiol. 2009; 71: 895–911. https://doi.org/10.1111/j.1365-2958.2008.06567.x PMID: 19170880

19. Kamper J, Kahmann R, Bolker M, Ma LJ, Brefort T, Saville BJ, et al. Insights from the genome of the biotrophic fungal plant pathogen Ustilago maydis. Nature. 2006; 444: 97–101. https://doi.org/10.1038/nature05248 PMID: 17080091

20. Vollmeister E, Schipper K, Baumann S, Haag C, Pohlmann T, Stock J, et al. Fungal development of the plant pathogen Ustilago maydis. FEMS Microbiol Rev. John Wiley & Sons, Ltd (10.1111); 2012; 36: 59–77. https://doi.org/10.1111/j.1574-6976.2011.00296.x PMID: 21729109

21. Matei A, Doehlemann G. Cell biology of corn smut disease—Ustilago maydis as a model for biotrophic interactions. Curr Opin Microbiol. Elsevier Ltd; 2016; 34: 60–66. https://doi.org/10.1016/j.mib.2016.07.020 PMID: 27504540

22. Lanver D, Tollot M, Schweizer G, Lo Presti L, Reissmann S, Ma L-S, et al. Ustilago maydis effectors and their impact on virulence. Nat Rev Microbiol. 2017; 15: 409–421. https://doi.org/10.1038/nrmicro.2017.33 PMID: 28479603

23. Redkar A, Matei A, Doehlemann G. Insights into Host Cell Modulation and Induction of New Cells by the Corn Smut Ustilago maydis. Front Plant Sci. Frontiers Media SA; 2017; 8: 899. https://doi.org/10.3389/fpls.2017.00899 PMID: 28611813

24. Flor-Parra I, Vranes M, Kamper J, Perez-Martin J. Biz1, a zinc finger protein required for plant invasion by Ustilago maydis, regulates the levels of a mitotic cyclin. Plant Cell. 2006; 18: 2369–2387. https://doi.org/10.1105/tpc.106.042754 PMID: 16905655

25. Bottin A, Kamper J, Kahmann R. Isolation of a carbon source-regulated gene from Ustilago maydis. Mol Gen Genet. 1996; 253: 342–52. https://doi.org/10.1007/pl00008601 PMID: 9003321

26. Djamei A, Schipper K, Rabe F, Ghosh A, Vincon V, Kahnt J, et al. Metabolic priming by a secreted fungal effector. Nature. 2011; 478: 395–398. https://doi.org/10.1038/nature10454 PMID: 21976020

27. Soberanes-Gutierrez C V, Juarez-Montiel M, Olguin-Rodriguez O, Hernandez-Rodriguez C, Ruiz-Herrera J, Villa-Tanaca L. The pep4 gene encoding proteinase A is involved in dimorphism and pathogenesis of Ustilago maydis. Mol Plant Pathol. 2015; 16: 837–46. https://doi.org/10.1111/mpp.12240 PMID: 25597948

28. Lanver D, Berndt P, Tollot M, Naik V, Vranes M, Warmann T, et al. Plant Surface Cues Prime Ustilago maydis for Biotrophic Development. PLoS Pathog. 2014; 10: e1004272. https://doi.org/10.1371/journal.ppat.1004272 PMID: 25033195

29. Bolker M, Bohnert HU, Braun KH, Gorl J, Kahmann R. Tagging pathogenicity genes in Ustilago maydis by restriction enzyme-mediated integration (REMI). Mol Gen Genet. Germany; 1995; 248: 547–552. https://doi.org/10.1007/bf02423450 PMID: 7476854

30. Banuett F, Herskowitz I. Different a alleles of Ustilago maydis are necessary for maintenance of filamentous growth but not for meiosis. Proc Natl Acad Sci U S A. 1989; 86: 5878–5882. https://doi.org/10.1073/pnas.86.15.5878 PMID: 16594058

31. Ali Khan H, Mutus B. Protein disulfide isomerase a multifunctional protein with multiple physiological roles. Front Chem. Frontiers Media SA; 2014; 2: 70. https://doi.org/10.3389/fchem.2014.00070 PMID: 25207270

32. Wilkinson B, Gilbert HF. Protein disulfide isomerase. Biochim Biophys Acta—Proteins Proteomics. 2004; 1699: 35–44. https://doi.org/10.1016/S1570-9639(04)00063-9

33. Breitenbach M, Weber M, Rinnerthaler M, Karl T, Breitenbach-Koller L. Oxidative stress in fungi: its function in signal transduction, interaction with plant hosts, and lignocellulose degradation. Biomolecules. 2015; 5: 318–342. https://doi.org/10.3390/biom5020318 PMID: 25854186

34. Banerjee S, Vishwanath P, Cui J, Kelleher DJ, Gilmore R, Robbins PW, et al. The evolution of N-glycan-dependent endoplasmic reticulum quality control factors for glycoprotein folding and degradation. Proc Natl Acad Sci. 2007; 104: 11676–11681. https://doi.org/10.1073/pnas.0704862104 PMID: 17606910

35. Lanver D, Muller AN, Happel P, Schweizer G, Haas FB, Franitza M, et al. The biotrophic development of Ustilago maydis studied by RNAseq analysis. Plant Cell. 2018; 30: tpc.00764.2017. https://doi.org/10.1105/tpc.17.00764 PMID: 29371439

36. Brefort T, Tanaka S, Neidig N, Doehlemann G, Vincon V, Kahmann R. Characterization of the largest effector gene cluster of Ustilago maydis. PLoS Pathog. 2014; 10: e1003866. https://doi.org/10.1371/journal.ppat.1003866 PMID: 24992561

37. Mares RE, Ramos MA. An amebic protein disulfide isomerase (PDI) complements the yeast PDI1 mutation but is unable to support cell viability under ER or thermal stress. FEBS Open Bio. 2018; 8: 49–55. https://doi.org/10.1002/2211-5463.12350 PMID: 29321956

38. Harries E, Gandia M, Carmona L, Marcos JF. The Penicillium digitatum protein O-mannosyltransferase Pmt2 is required for cell wall integrity, conidiogenesis, virulence and sensitivity to the antifungal peptide PAF26. Mol Plant Pathol. 2015; 16: 748–61. https://doi.org/10.1111/mpp.12232 PMID: 25640475

39. Guo M, Tan L, Nie X, Zhu X, Pan Y, Gao Z. The Pmt2p-Mediated Protein O-Mannosylation Is Required for Morphogenesis, Adhesive Properties, Cell Wall Integrity and Full Virulence of Magnaporthe oryzae. Front Microbiol. 2016; 7: 630. https://doi.org/10.3389/fmicb.2016.00630 PMID: 27199956

40. Gonzalez M, Brito N, Frias M, Gonzalez C. Botrytis cinerea Protein O-Mannosyltransferases Play Critical Roles in Morphogenesis, Growth, and Virulence. Yu J-H, editor. PLoS One. 2013; 8: e65924. https://doi.org/10.1371/journal.pone.0065924 PMID: 23762450

41. Wagener J, Weindl G, de Groot PWJ, de Boer AD, Kaesler S, Thavaraj S, et al. Glycosylation of Candida albicans cell wall proteins is critical for induction of innate immune responses and apoptosis of epithelial cells. Lenz LL, editor. PLoS One. 2012; 7: e50518. https://doi.org/10.1371/journal.pone.0050518 PMID: 23226301

42. Willger SD, Ernst JF, Alspaugh JA, Lengeler KB. Characterization of the PMT gene family in Cryptococcus neoformans. Lin X, editor. PLoS One. 2009; 4: e6321. https://doi.org/10.1371/journal.pone.0006321 PMID: 19633715

43. Leach MD, Brown AJP. Posttranslational Modifications of Proteins in the Pathobiology of Medically Relevant Fungi. Eukaryot Cell. 2012; 11: 98–108. https://doi.org/10.1128/EC.05238-11 PMID: 22158711

44. Uhse S, Djamei A. Effectors of plant-colonizing fungi and beyond. Zipfel C, editor. PLOS Pathog. 2018; 14: e1006992. https://doi.org/10.1371/journal.ppat.1006992 PMID: 29879221

45. Xie X, Lipke PN. On the evolution of fungal and yeast cell walls. Yeast. 2010; 27: 479–488. https://doi.org/10.1002/yea.1787 PMID: 20641026

46. Kruszewska JS, Perlińska-Lenart U, Górka-Nieć W, Orłowski J, Zembek P, Palamarczyk G. Alterations in protein secretion caused by metabolic engineering of glycosylation pathways in fungi. Acta Biochim Pol. 2008; 55: 447–56. PMID: 18797519

47. Nielsen H. Predicting Secretory Proteins with SignalP. Methods in molecular biology (Clifton, NJ). 2017. pp. 59–73. https://doi.org/10.1007/978-1-4939-7015-5_6 PMID: 28451972

48. Sperschneider J, Dodds PN, Singh KB, Taylor JM. ApoplastP: prediction of effectors and plant proteins in the apoplast using machine learning. New Phytol. 2018; 217: 1764–1778. https://doi.org/10.1111/nph.14946 PMID: 29243824

49. Sperschneider J, Gardiner DM, Dodds PN, Tini F, Covarelli L, Singh KB, et al. Effector P: predicting fungal effector proteins from secretomes using machine learning. New Phytol. 2016; 210: 743–761. https://doi.org/10.1111/nph.13794 PMID: 26680733

50. Burggraaf A-M, Punt PJ, Ram AFJ. The unconventional secretion of PepN is independent of a functional autophagy machinery in the filamentous fungus Aspergillus niger. FEMS Microbiol Lett. 2016; 363. https://doi.org/10.1093/femsle/fnw152 PMID: 27284019

51. Koepke J, Kaffarnik F, Haag C, Zarnack K, Luscombe NM, Konig J, et al. The RNA-Binding Protein Rrm4 is Essential for Efficient Secretion of Endochitinase Cts1. Mol Cell Proteomics. 2011; 10: M111.011213. https://doi.org/10.1074/mcp.M111.011213 PMID: 21808052

52. Stock J, Sarkari P, Kreibich S, Brefort T, Feldbrugge M, Schipper K. Applying unconventional secretion of the endochitinase Cts1 to export heterologous proteins in Ustilago maydis. J Biotechnol. 2012; 161: 80–91. https://doi.org/10.1016/j.jbiotec.2012.03.004 PMID: 22446315

53. Aschenbroich J, Hussnaetter KP, Stoffels P, Langner T, Zander S, Sandrock B, et al. The germinal centre kinase Don3 is crucial for unconventional secretion of chitinase Cts1 in Ustilago maydis. Biochim Biophys Acta—Proteins Proteomics. 2018; https://doi.org/10.1016/j.bbapap.2018.10.007 PMID: 30316861

54. Paper JM, Scott-Craig JS, Adhikari ND, Cuomo CA, Walton JD. Comparative proteomics of extracellular proteins in vitro and in planta from the pathogenic fungus Fusarium graminearum. Proteomics. 2007; 7: 3171–83. https://doi.org/10.1002/pmic.200700184 PMID: 17676664

55. Lanver D, Mendoza-Mendoza A, Brachmann A, Kahmann R. Sho1 and Msb2-related proteins regulate appressorium development in the smut fungus Ustilago maydis. Plant Cell. 2010; 22: 2085–2101. https://doi.org/10.1105/tpc.109.073734 PMID: 20587773

56. Tollot M, Assmann D, Becker C, Altmuller J, Dutheil JY, Wegner C-E, et al. The WOPR Protein Ros1 Is a Master Regulator of Sporogenesis and Late Effector Gene Expression in the Maize Pathogen Ustilago maydis. Wang Y, editor. PLoS Pathog. 2016; 12: e1005697. https://doi.org/10.1371/journal.ppat.1005697 PMID: 27332891

57. Wahl R, Zahiri A, Kamper J. The Ustilago maydis b mating type locus controls hyphal proliferation and expression of secreted virulence factors in planta. Mol Microbiol. 2010; 75: 208–220. https://doi.org/10.1111/j.1365-2958.2009.06984.x PMID: 19943901

58. Skibbe DS, Doehlemann G, Fernandes J, Walbot V. Maize tumors caused by Ustilago maydis require organ-specific genes in host and pathogen. Science (80-). 2010; 328: 89–92. https://doi.org/10.1126/science.1185775 PMID: 20360107

59. Zhou X, Liu W, Wang C, Xu Q, Wang Y, Ding S, et al. A MADS-box transcription factor MoMcm1 is required for male fertility, microconidium production and virulence in Magnaporthe oryzae. Mol Microbiol. 2011; 80: 33–53. https://doi.org/10.1111/j.1365-2958.2011.07556.x PMID: 21276092

60. Pan Y, Pan R, Tan L, Zhang Z, Guo M. Pleiotropic roles of O-mannosyltransferase MoPmt4 in development and pathogenicity of Magnaporthe oryzae. Curr Genet. 2018; https://doi.org/10.1007/s00294-018-0864-2 PMID: 29946987

61. Li M, Liu X, Liu Z, Sun Y, Liu M, Wang X, et al. Glycoside Hydrolase MoGls2 Controls Asexual/Sexual Development, Cell Wall Integrity and Infectious Growth in the Rice Blast Fungus. Wang Z, editor. PLoS One. 2016; 11: e0162243. https://doi.org/10.1371/journal.pone.0162243 PMID: 27607237

62. Fernandez-Alvarez A, Elias-Villalobos A, Ibeas JI. The requirement for protein O-mannosylation for Ustilago maydis virulence seems to be linked to intrinsic aspects of the infection process rather than an altered plant response. Plant Signal Behav. 2010; 5: 412–414. https://doi.org/10.4161/psb.5.4.10805 PMID: 20061799

63. Win J, Chaparro-Garcia A, Belhaj K, Saunders DGO, Yoshida K, Dong S, et al. Effector Biology of Plant-Associated Organisms: Concepts and Perspectives. Cold Spring Harb Symp Quant Biol. 2012; 77: 235–247. https://doi.org/10.1101/sqb.2012.77.015933 PMID: 23223409

64. Seitner D, Uhse S, Gallei M, Djamei A. The core effector Cce1 is required for early infection of maize by Ustilago maydis. Mol Plant Pathol. 2018; 19: 2277–2287. https://doi.org/10.1111/mpp.12698 PMID: 29745456

65. Trombetta ES, Parodi AJ. Quality Control and Protein Folding in the Secretory Pathway. Annu Rev Cell Dev Biol. 2003; 19: 649–676. https://doi.org/10.1146/annurev.cellbio.19.110701.153949 PMID: 14570585

66. Moremen KW, Molinari M. N-linked glycan recognition and processing: the molecular basis of endoplasmic reticulum quality control. Curr Opin Struct Biol. 2006; 16: 592–9. https://doi.org/10.1016/j.sbi.2006.08.005 PMID: 16938451

67. Marschall R, Tudzynski P. The Protein Disulfide Isomerase of Botrytis cinerea: An ER Protein Involved in Protein Folding and Redox Homeostasis Influences NADPH Oxidase Signaling Processes. Front Microbiol. Frontiers Media SA; 2017; 8: 960. https://doi.org/10.3389/fmicb.2017.00960 PMID: 28611757

68. Doehlemann G, van der Linde K, Assmann D, Schwammbach D, Hof A, Mohanty A, et al. Pep1, a secreted effector protein of Ustilago maydis, is required for successful invasion of plant cells. PLoS Pathog. 2009; 5: e1000290. https://doi.org/10.1371/journal.ppat.1000290 PMID: 19197359

69. Hemetsberger C, Herrberger C, Zechmann B, Hillmer M, Doehlemann G. The Ustilago maydis effector Pep1 suppresses plant immunity by inhibition of host peroxidase activity. PLoS Pathog. 2012; 8: e1002684. https://doi.org/10.1371/journal.ppat.1002684 PMID: 22589719

70. Mueller AN, Ziemann S, Treitschke S, Assmann D, Doehlemann G. Compatibility in the Ustilago maydis-maize interaction requires inhibition of host cysteine proteases by the fungal effector Pit2. PLoS Pathog. 2013; 9: e1003177. https://doi.org/10.1371/journal.ppat.1003177 PMID: 23459172

71. Redkar A, Hoser R, Schilling L, Zechmann B, Krzymowska M, Walbot V, et al. A Secreted Effector Protein of Ustilago maydis Guides Maize Leaf Cells to Form Tumors. Plant Cell. 2015; 27: 1332–1351. https://doi.org/10.1105/tpc.114.131086 PMID: 25888589

72. Sambrook J, Frisch E, Maniatis T. Molecular cloning: a laboratory manual, 2nd ed. 2nd ed. Cold Spring Harbor, NY: Cold Spring Harbor Laboratory Press; 1989.

73. Gillissen B, Bergemann J, Sandmann C, Schroeer B, Bolker M, Kahmann R. A two-component regulatory system for self/non-self recognition in Ustilago maydis. Cell. 1992; 68: 647–657. https://doi.org/10.1016/0092-8674(92)90141-x PMID: 1739973

74. Schulz B, Banuett F, Dahl M, Schlesinger R, Schafer W, Martin T, et al. The b alleles of U. maydis, whose combinations program pathogenic development, code for polypeptides containing a homeodomain-related motif. Cell. 1990; 60: 295–306. https://doi.org/10.1016/0092-8674(90)90744-y PMID: 1967554

75. Brachmann A, Konig J, Julius C, Feldbrugge M. A reverse genetic approach for generating gene replacement mutants in Ustilago maydis. Mol Genet Genomics. 2004; 272: 216–226. https://doi.org/10.1007/s00438-004-1047-z PMID: 15316769

76. Fuchs U, Hause G, Schuchardt I, Steinberg G. Endocytosis is essential for pathogenic development in the corn smut fungus Ustilago maydis. Plant Cell. 2006; 18: 2066–81. https://doi.org/10.1105/tpc.105.039388 PMID: 16798890

77. Wedlich-Soldner R, Bolker M, Kahmann R, Steinberg G. A putative endosomal t-SNARE links exo- and endocytosis in the phytopathogenic fungus Ustilago maydis. Embo J. 2000; 19: 1974–1986. https://doi.org/10.1093/emboj/19.9.1974 PMID: 10790364

78. Pitarch A, Sanchez M, Nombela C, Gil C. Sequential fractionation and two-dimensional gel analysis unravels the complexity of the dimorphic fungus Candida albicans cell wall proteome. Mol Cell Proteomics. 2002; 1: 967–982. https://doi.org/10.1074/mcp.m200062-mcp200 PMID: 12543933

79. Theisen U, Straube A, Steinberg G. Dynamic rearrangement of nucleoporins during fungal "open" mitosis. Mol Biol Cell. 2008; 19: 1230–40. https://doi.org/10.1091/mbc.E07-02-0130 PMID: 18172026